ADVANCED MATERIALS
www.advmat.de

Toward Electrocatalytic Methanol Oxidation Reaction: Longstanding Debates and Emerging Catalysts

*Jianmei Wang, Bingxing Zhang, Wei Guo, Lei Wang, Jian Chen, Hongge Pan, and Wenping Sun**

The study of direct methanol fuel cells (DMFCs) has lasted around 70 years, since the first investigation in the early 1950s. Though enormous effort has been devoted in this field, it is still far from commercialization. The methanol oxidation reaction (MOR), as a semi-reaction of DMFCs, is the bottleneck reaction that restricts the overall performance of DMFCs. To date, there has been intense debate on the complex six-electron reaction, but barely any reviews have systematically discussed this topic. To this end, the controversies and progress regarding the electrocatalytic mechanisms, performance evaluations as well as the design science toward MOR electrocatalysts are summarized. This review also provides a comprehensive introduction on the recent development of emerging MOR electrocatalysts with a focus on the innovation of the alloy, core–shell structure, heterostructure, and single-atom catalysts. Finally, perspectives on the future outlook toward study of the mechanisms and design of electrocatalysts are provided.

1. Introduction

Compared to H_2, methanol can be easily handled and distributed via the existing infrastructure for gasoline. In this regard, the direct methanol fuel cell (DMFC) can be applied as a promising electrochemical power source and triggered intense research interests since the early 1950s.[1] The theoretical energy density of DMFCs is 6.13 kW h kg^{-1}, which is tenfold higher than that of lithium-ion batteries.[2,3] Furthermore, the volumetric energy density of methanol is around 17.28 MJ L^{-1}, several times higher than that of H_2 (1.9 MJ L^{-1} at 20 MPa, 4.7 MJ L^{-1} for liquid H_2).[4,5] In DMFCs, methanol is oxidized at the anode, producing CO_2, H^+, and e^- (methanol oxidation reaction (MOR): $CH_3OH + H_2O \rightarrow CO_2 + 6H^+ + 6e^-$). At the cathode, O_2 combines with H^+ and e^-, being reduced into H_2O (oxygen reduction reaction (ORR): $O_2 + 4H^+ + 4e^- \rightarrow 2H_2O$).[6] It should be noted that the ORR as a key reaction in fuel cells and metal–air batteries, has a relatively mature development.[7–10] In contrast, the poor stability and sluggish kinetics make MOR become the bottleneck of DMFCs and restrict their commercialization.[11–13]

The thermodynamic equilibrium potential for MOR is 0.04 V, which means the theoretical output potential is around 1.2 V for a standard methanol/oxygen fuel cell.[14] Although the equilibrium potential for CH_3OH oxidation to CO_2 is very close to that of H_2 oxidation, the rate of the MOR is slowed down by multi-step reaction pathways. Pt-based (active in both acid and basic solution) and Pd-based (only active in basic solution) materials are the main active electrocatalysts for the MOR (**Figure 1**). Usually, Pt- and Pd-based catalysts demand the onset potential of around 450 and 550 mV (versus reversible hydrogen electrode (RHE)) to trigger the MOR, respectively.[15] A number of non-noble-metal catalysts have also been reported to be active toward the MOR, but the high MOR onset potential makes them impractical in DMFCs.[5,16–18] Nevertheless, these non-noble metal-based materials have been proposed to catalyze MOR for replacing the more sluggish anodic oxygen evolution reaction in electrolyzer for hydrogen generation, and in many cases, value-added products (e.g., formate) can be obtained.[5,19,20] Overall, the Pt group metal based MOR electrocatalysts seem to be the only choice for DMFCs. Unfortunately, their application is stifled by the high cost, sluggish kinetics, and poisoning issues. Since more than 95% of the noble metal is recoverable at the end of a fuel cell life,[21] how to conquer the limited catalytic behaviors is more challenging than the price issue for DMFCs as promising green power conversion devices.

Although significant efforts have been devoted to designing high-performance MOR electrocatalysts, their development is still lagging far behind. Herein, we aim to give a

J. Wang, B. Zhang, W. Guo, H. Pan, W. Sun
School of Materials Science and Engineering
Zhejiang University
Hangzhou 310058, P. R. China
E-mail: wenpingsun@zju.edu.cn

L. Wang
Department of Chemical and Biomolecular Engineering
National University of Singapore
Singapore 117585, Singapore

J. Chen, H. Pan
Institute of Science and Technology for New Energy
Xi'an Technological University
Xi'an 710021, P. R. China

W. Sun
State Key Laboratory of Clean Energy Utilization
Zhejiang University
Hangzhou 310027, P. R. China

The ORCID identification number(s) for the author(s) of this article can be found under https://doi.org/10.1002/adma.202211099

DOI: 10.1002/adma.202211099

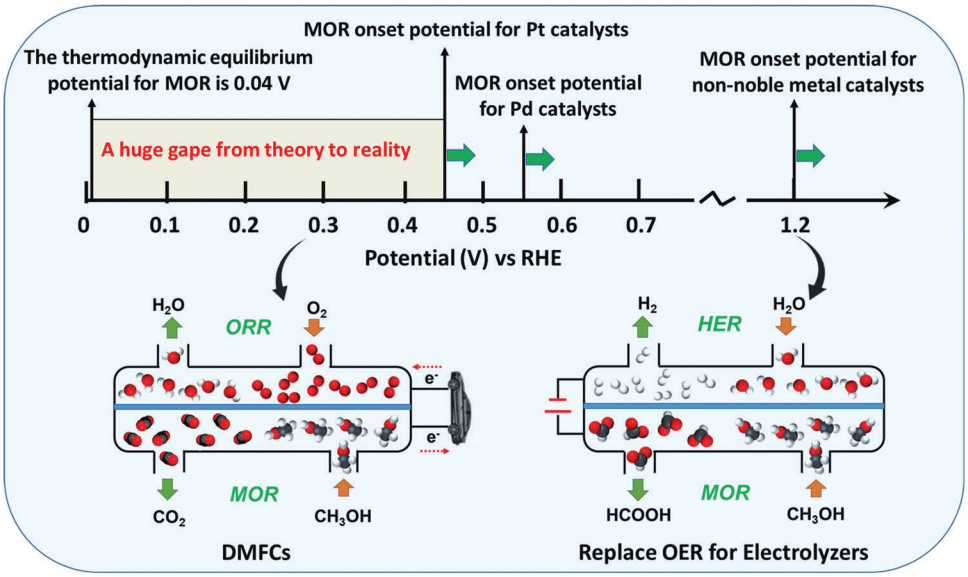

Figure 1. Illustration for the Pt-, Pd-, and non-noble-metal-based MOR catalysts and their corresponding applications. HER: hydrogen evolution reaction.

comprehensive review on the longstanding debates and the evolution of the advanced catalysts toward the MOR. Recent development and limitations of the catalytic mechanisms are first introduced. Afterward, the controversial criteria to evaluate the durability and anti-CO ability of electrocatalysts are discussed. We then focus on the recent progress of advanced MOR electrocatalysts: from nanosized to single-atom ones. The evolution of the emerging alloy, core–shell, and heterostructured catalysts is highlighted. For single-atom catalysts (SACs), the debates on their capabilities toward the MOR and the current developments are systematically discussed. Finally, perspectives on the challenges and opportunities of the mechanism study and electrocatalysts design are emphasized.

2. Development and Limitations of the MOR Mechanism

The rational design and synthesis of MOR electrocatalysts should rely on a thorough understanding of the reaction mechanism. However, in the last 10 years, most efforts have been focused on the design of advanced MOR electrocatalysts, and the understanding of corresponding mechanisms still mainly owes to pioneering works from 20 years ago. Therefore, in this section, the development and limitations of the MOR mechanisms will be introduced to provide deep insights for propelling its further development.

2.1. Methanol Oxidation Pathway

Though the exploration of MOR has a history of around a century, its electrocatalytic mechanism was uncovered till the 1980s with the development of in situ infrared spectroscopy and mass-spectrometry-related techniques such as differential electrochemical mass spectrometry (DEMS).[22] Based on the collected chemical information of adsorbates and intermediates in the processes of the MOR, a well-accepted dual-pathway mechanism was raised (**Figure 2**). In detail, the MOR, ideally involving six-electron transfer, proceeds via either a CO pathway or a CO-free pathway, as shown in Figure 2.

In the CO pathway (indirect pathway), CO* is formed after the deprotonation of COH* or CHO* (red arrows). Then CO* combines with a surface hydroxyl (OH*, blue highlighted in Figure 2) and converts to COOH*, which is further oxidized to CO_2. It should be noted that the OH* is from water dissociation in the acid solution and OH^- ions in the basic solution.[23] In the CO-free pathway or direct pathway, instead of direct deprotonation, the possible intermediates like CHO*, COH*, or CH_2O* would interact with OH* to form CHOOH*, $C(OH)_2$*, or H_2COOH*, respectively. These di-oxygenated species then go dehydrogenation to produce CO_2 through either COOH* or CHOO*.[24] Notably, two different viewpoints regarding the formation of $HCOOCH_3$ are proposed by researchers: 1) from the homogeneous reaction between CHOOH* and CH_3OH;[25,26] 2) from the nucleophilic attack of the CH_3OH on CHO*.[27] In alkaline media, the easier formation of OH* would efficiently remove the adsorbed carbonous species and result in faster kinetics. However, the inevitable precipitation of formed carbonate or bicarbonate in the catalyst pores and the induced pH changes would result in a gradual activity decay for DMFCs operating under alkaline media.[24,28,29]

Among all the possible intermediates, CO* is the most stable one, which could block the active sites and prevent the proceeding of the reaction at low potentials.[30] Yet no catalysts have ever thoroughly conquered the anode poisoning problem. Normally, changing the binding energies (BEs) of different intermediates to lower the further oxidation barrier of CO* or switching the reaction to a CO-free dominated pathway are the most commonly applied strategies to solve the CO poisoning issues. However, to the best of our knowledge, no clear BE-reaction relation has been established yet stemming from their complex adsorption energy scaling relations (please check Section 5.1 for the

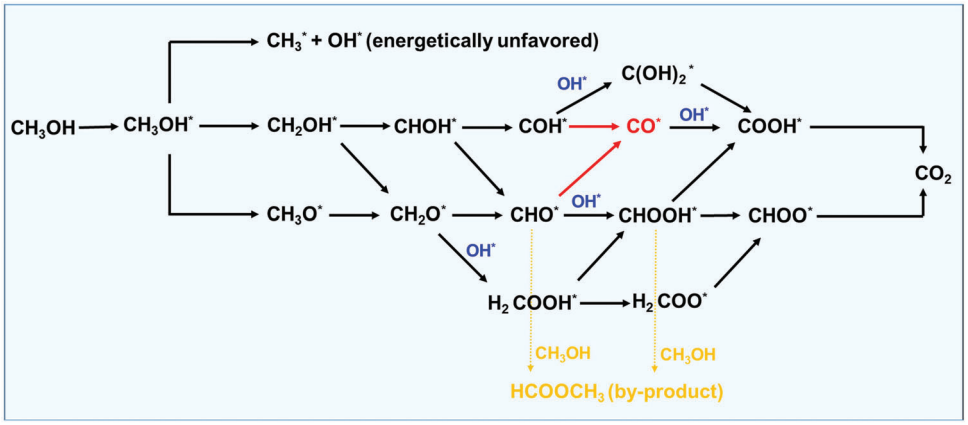

Figure 2. A dual-pathway mechanism for electrocatalytic MOR, where * represents the adsorption site on the catalyst surface, the red arrows indicate the CO pathway, and the others the CO-free pathway.

details).[31] Moreover, the specific relationship of the methanol oxidation pathway with potential, solution, catalyst, and OH* remains largely elusive which will be discussed in the following section.

2.2. Limitations of Current Theory Investigations

Whether the dual-pathway mechanism only happens at high potentials on a platinum electrode is very controversial but is of significant importance. Stuve's group observed CO_2 production on both Pt (100)[32] and Pt (111)[33] from 0.5 to 0.65 V (vs RHE) where the adsorbed CO is quite stable, and they claimed the formed CO_2 was from the CO-free pathway. Conversely, Wieckowski and coworkers argued that a dual pathway occurs at abovementioned "CO stable" potential range and the sole CO pathway happens at even lower potentials.[31] Chronoamperometry (CA), fast scan cyclic voltammetry (CV) and theoretical methods were applied to study the effect of potential on the MOR pathway. They defined a parameter r, which equals Q_{CA}/Q_{CV}. Q_{CA} is the MOR charge obtained from the CA test and Q_{CV} is the charge obtained from the oxidation of CO* which is obtained from the fast scan CV test. They assumed that in the tested potential range, all the CO* remained on the electrode surface. When $r = 2$, the sole CO pathway occurs and $r > 2$ means the existence of a dual-path mechanism. **Figure 3**a displays that the sole CO pathway happens at the potential from 0.2–0.4 V (vs RHE) for Pt (100) and below 0.35 V for Pt (111) and Pt (110). Chen et al. also reported similar results that the contribution of the CO pathway to CO_2 production decreased as the potential increased from 0.6 to 0.75 V (vs RHE) on a Pt film electrode, as revealed by the coupled DEMS and electrochemical attenuated-total-reflectance Fourier transform infrared (ATR-FTIR) spectroscopy results.[30] It can be concluded from these studies that the contribution of the CO-free pathway is more significant at high potentials and the oxidation mechanism is also surface structure-dependent. Unraveling the dominant pathway is of significant importance because if the reaction proceeds via the CO pathway, further catalyst design should focus on destabilizing CO*. If, instead, further research should attempt to improve the kinetics and selectivity of the CO-free pathway. With the development of advanced techniques, deeper mechanism understanding is more accessible and requires specific attention.

Moreover, it is also recognized that solvent effects may play a role in the dual-pathway mechanism, though it is not completely understood yet. Batista and co-workers found that a much higher MOR current density can be obtained in $HClO_4$ than in H_2SO_4 solution for Pt (111) (Figure 3b).[34] After electrolysis of 1.0 M methanol on Pt (111) under 0.6 V for 15 min, around 0.028 μmol HCHO, 0.0047 μmol HCOOH, and 0.039 μmol CO_2 were detected in 0.1 M $HClO_4$, and around 0.027 μmol HCHO, 0.0044 μmol HCOOH, and 0.0017 μmol CO_2 were detected in 0.5 M H_2SO_4 (Figure 3c). The production of HCHO and HCOOH is practically the same in both electrolytes but the CO_2 yield greatly increases in $HClO_4$. Therefore, the authors concluded that the methanol is mainly oxidized via the CO-free pathway (through soluble intermediates) in H_2SO_4 but is mainly via the CO-pathway (without the production of HCHO and HCOOH) in $HClO_4$ solution. The adsorption of SO_4^{2-} ions on Pt (111) is much stronger than that of ClO_4^- ions, which not only influence the catalytic behavior but also inhibit the CO-pathway.[35] The results were also evidenced by Lai et al.[36] Undeniable, the anion adsorption would possibly influence the reaction pathway, but Varela and co-workers reported that the anion adsorption affects the CO-free pathway more significantly under oscillatory regimes, as evidenced by the results from on line DEMS.[37]

Additionally, Zeng et al. proved that the dual-pathway mechanism is Pt lattice strain-dependent.[38] They prepared a series of Pt–Fe–Cu ternary ordered intermetallics ($PtFeCu_0$/C, $PtFe_{0.7}Cu_{0.3}$/C, $PtFe_{0.5}Cu_{0.5}$/C) and found that the CO-free pathway increases monotonically with the increase in the lattice contraction of Pt. It was assumed that the strained Pt lattice favors the stabilization of the transition-state intermediates in the CO-free pathway. The induced lattice strains enable the alteration of electronic structures of catalysts, which would result in significant weakening or strengthening of their adsorption properties and further lead to the change of the reaction pathway.[39] It is essential to screen the optimal strain-modified catalysts for an improved MOR performance, which is discussed in detail in Section 4.2.

The conclusion about the effect of co-catalysts and the function of OH* is still ambiguous due to the lack of direct evidence. For

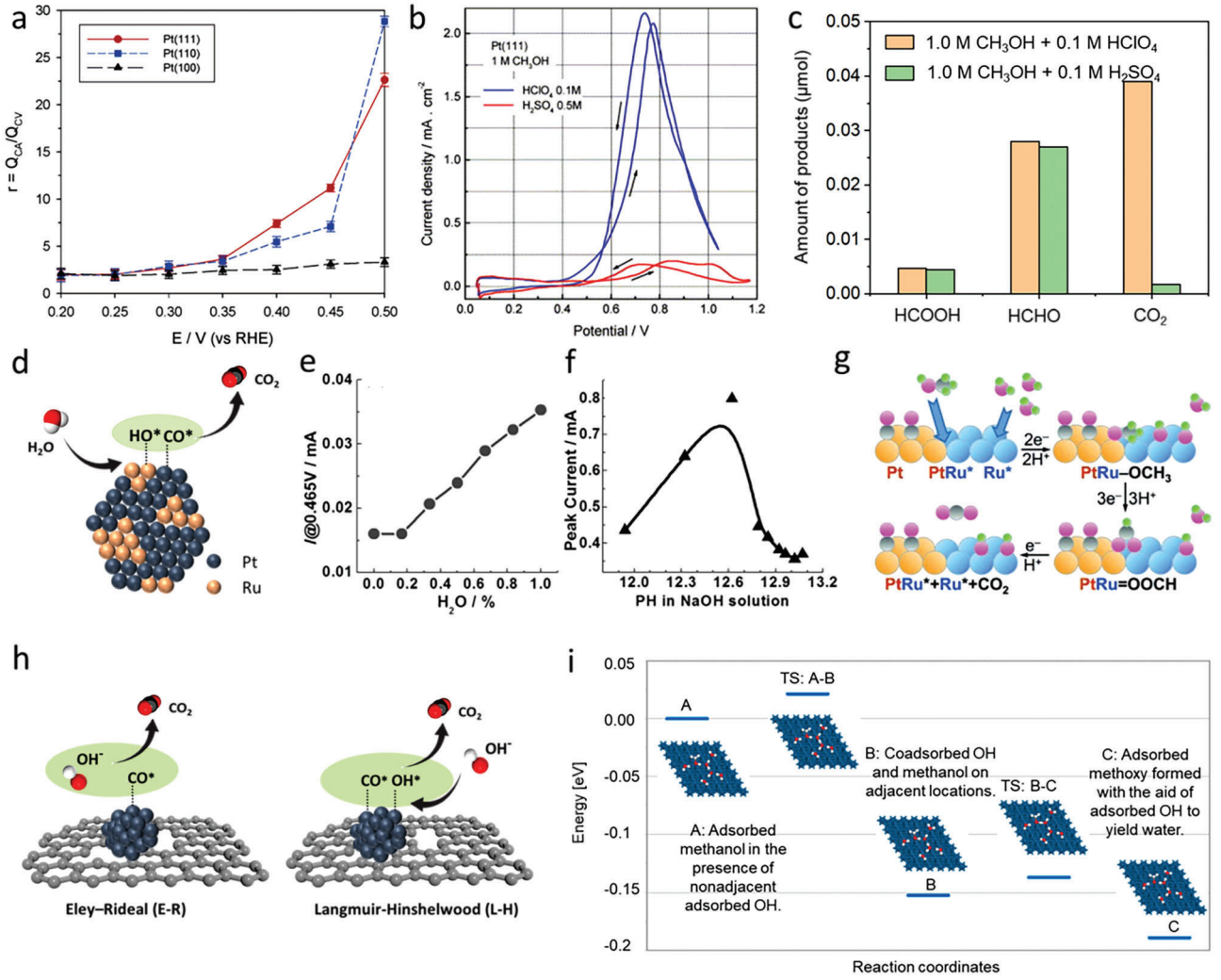

Figure 3. a) Plots of *r* as a function of the applied potential in 0.1 M H_2SO_4 and 0.1 M CH_3OH. Reproduced with permission.[31] Copyright 2005, American Chemical Society. b) CV for MOR at Pt (111) in 1 M CH_3OH with 0.1 M $HClO_4$ or 0.5 M H_2SO_4, respectively. c) Products amount obtained at 0.6 V on a Pt (111) electrode in 1 M CH_3OH with 0.1 M $HClO_4$ or 0.5 M H_2SO_4, respectively. b) Reproduced with permission.[34] Copyright 2003, Elsevier. (c) is plotted based on the data obtained from Table 1 in ref. [34]. d) Schematic illustration of the classical bifunctional mechanism of PtRu alloy. e) The CA currents collected at 0.465 V as a function of the H_2O/H_2O+D_2O ration on the PtRu. f) The MOR peak current of PtRu as a function of pH values. g) The revised MOR bifunctional mechanism on PtRu. e–g) Reproduced with permission.[43] Copyright 2015, Wiley-VCH. h) Schematic illustration of E–R/L–H theory for MOR. i) Energy profiles for methanol activation on the Pt (111) surface with different states of OH, TS: transition states. i) Reproduced with permission.[52] Copyright 2022, American Chemical Society.

example, the bifunctional mechanism is a widely accepted theorem to guide the design of advanced MOR catalysts. This mechanism gives the idea that the introduction of oxophilic species can facilitate the removal of poisoning carbonaceous intermediates via promoting the adsorption of OH* at a lower potential (Figure 3d). Take the traditional PtRu alloy as an example, the synergistic effect of these two metals can be stated in the following equation:

$$Pt - CO + HO - Ru \rightarrow Pt^* + Ru^* + CO_2 + H^+ + e^- \quad (1)$$

The bifunctional mechanism has been supported by much strong circumstantial evidence but lacks direct molecular-level evidence.[40–42] Tong et al. proposed a different conclusion based on the results from ATR surface-enhanced infrared absorption spectroscopy (ATR-SEIRAS), DMFC, and isotope-labeling studies.[43] They found that the performance enhancement of PtRu in MOR was not accompanied by easier elimination of the CO* and surprisingly, formate was detected as the reaction intermediate. When the MOR activity was plotted as a function of the ratio of $H_2O/(H_2O + D_2O)$ (Figure 3e) and the pH values in alkaline environment (Figure 3f), it was found that the formation of Ru–OH still plays an important role in the MOR catalytic process of PtRu catalysts. Based on the above observations, they proposed a revised bifunctional mechanism that, instead of facilitating the removal of CO*, the presence of the Ru in PtRu systems selectively enhances the CO-free pathway, and the corresponding reactions are shown below (Figure 3g):

$$Ru^{*} + H_2O \rightarrow Ru - OH + H^{+} + e^{-} \quad (2)$$

$$PtRu^{*} + CH_3OH \rightarrow PtRu - OCH_3 + H^{+} + e^{-} \quad (3)$$

$$PtRu - OCH_3 + Ru - OH \rightarrow PtRu = OOCH + Ru^{*} + 3(H^{+} + e^{-}) \quad (4)$$

$$PtRu = OOCH \rightarrow PtRu^{*} + CO_2 + H^{+} + e^{-} \quad (5)$$

In follow-up studies, Cai and co-workers also proved that the enhanced MOR performance of SnO_2-modified Pt originates from the revised bifunctional mechanism (selectively enhancing the CO-free pathway).[44] Whereas, the classical bifunctional mechanism (accelerate the CO removal) is still the mainstream no matter in the advanced PtRu catalysts or other oxophilic-species-modified Pt systems.[45–49] In our opinion, the bifunctional mechanism or "revised bifunctional mechanism" may be true under certain conditions, while it might fail to elucidate another system. More advanced in situ and operando characterization techniques should be applied to verify the proposed mechanism as highlighted in Section 5.1.

It is also well-accepted that the electrocatalytic MOR starts from C–H or O–H bond scissions and forms either CH_2OH^{*} or CH_3O^{*} and the role of OH is believed to oxidize specific adsorbed carbonaceous intermediates (Figure 2). In acidic electrolytes, due to the deficiency of OH^{-} ions, the OH from water dissociation should first adsorb on the active sites to take part in the reaction via the Langmuir–Hinshelwood (L–H) way. In alkaline electrolytes, it is believed that besides L–H mechanism, the abundant OH^{-} ions are able to participate in the reaction through the Eley–Rideal (E–R) mechanism (Figure 3h).[23,50,51] Very recently, Mekazni et al. came up with different views that on platinum, MOR only takes place with the presence of OH* and the O–H bond of methanol would always break in the first place, producing H_3CO^{*}.[52] They claimed that the OH* is involved in the mechanism rather than only oxidizing the already existing CO*, because it was found that CO* from MOR is only formed when OH* is already present on the electrode surface. The DFT calculations show that the adsorption of methanol on Pt (111) is significantly favored with the assistance of OH* and the nonadjacent OH* will quickly transit to the most favorable co-adsorbed location (Figure 3i). Moreover, the presence of OH* favors the scission of the O–H bond instead of the C–H bond because the C–H bond is less polarized. If this proposal can be further evidenced and accepted, the understanding of MOR will be renewed from at least two aspects: 1) the E–R mechanism does not exist in MOR because OH^{-} ions cannot directly participate in the reaction; 2) the adsorbed OH should always be considered when conducting DFT calculations. However, most of the abovementioned experimental and theoretical results were obtained based on single-crystal electrodes. The case is more complicated in polycrystalline catalysts, since the behaviors of different catalyst facets differ significantly, but have been rarely studied yet.

In practical cases, the rate-determining step (RDS) of MOR for a specific electrocatalyst also remains inconclusive. Take Pt as an example, whose RDS depends on the exposed facets.[26,53] According to the difference of the Tafel range for MOR, Herrero and coworkers suggested the first C–H bond splitting from CH_3OH^{*} to CH_2OH^{*} is the RDS in MOR on Pt (111) and (110) surfaces, while the C–H bond break of CH_2OH^{*} is the RDS for Pt (100).[54] However, Stuve's group applied a L–H kinetic model and indicated the dehydrogenation of either adsorbed HCOO or adsorbed COOH is the RDS for Pt (111) and the CO oxidation is the RDS for Pt (100).[55] More recent computational studies also revealed that the overall MOR activity was determined by the removal of CO for the Pt (100) surface with[56] or without[57] tensile strains. In addition, Farias et al. applied isotope labeling and in situ FTIR techniques proving that even for the same exposed facet, step sites and terrace sites show different methanol electrooxidation pathways.[58]

It has to be mentioned that in some cases, researchers place much reliance on the DFT calculations to explore the MOR pathways of the designed catalysts. However, the mechanism of methanol decomposition could be different between ultrahigh vacuum and electrochemical reaction environments.[59] Moreover, due to the complexity of electrochemistry, the RDS may change accordingly with the process of reaction.[60] Thus, it is almost impossible for DFT calculations to simulate the real electrochemical conditions with the consideration of all the effects such as local pH values, methanol concentrations, solution ions, electric field differences, and the evolution of the electrode/solution interface during the reaction. Therefore, DFT calculations should always couple with rigorous experimental verification to uncover the science behind relevant experiments. With regard to the catalyst design, current efforts are mainly focused on lowering the oxidation barrier of CO* or switching the reaction to a CO-free dominated pathway. From the perspective of the d-band center theory, the engineered electronic structures of electrocatalysts are expected to regulate the BEs of the adsorbates on the active sites which can finally lead to different reactivity.[61–63] Typically, alloying, inducing strain, and tuning the interaction at heterostructured interfaces are the most efficient strategies applied to regulate the d-band center of electrocatalysts. In addition, different components from a heterostructured electrocatalyst may also favor the MOR by the synergistic effect. The recent development of advanced MOR electrocatalysts will be discussed in Section 4.

3. Controversial Criteria

In the lab, a three-electrode system is usually used to replace the tedious membrane electrode assembly (MEA) for rapidly evaluating and screening a given MOR electrocatalyst. Mass activity (MA), specific activity (SA), overpotential, anti-poisoning capability, selectivity, and stability are well-accepted criteria to evaluate the electrocatalysts. Here, we only discuss the highly controversial criteria used to estimate the anti-poisoning capability and stability of MOR electrocatalysts. Also, we would like to stress the importance of the characterization of electrocatalysts during tests and the qualitative analysis of reaction products at the end of this section.

3.1. I_f/I_b for Evaluating the CO Anti-Poisoning Capability

There are two oxidation peaks in a typical CV of methanol electrooxidation (**Figure 4**a). The current ratio of these two peaks

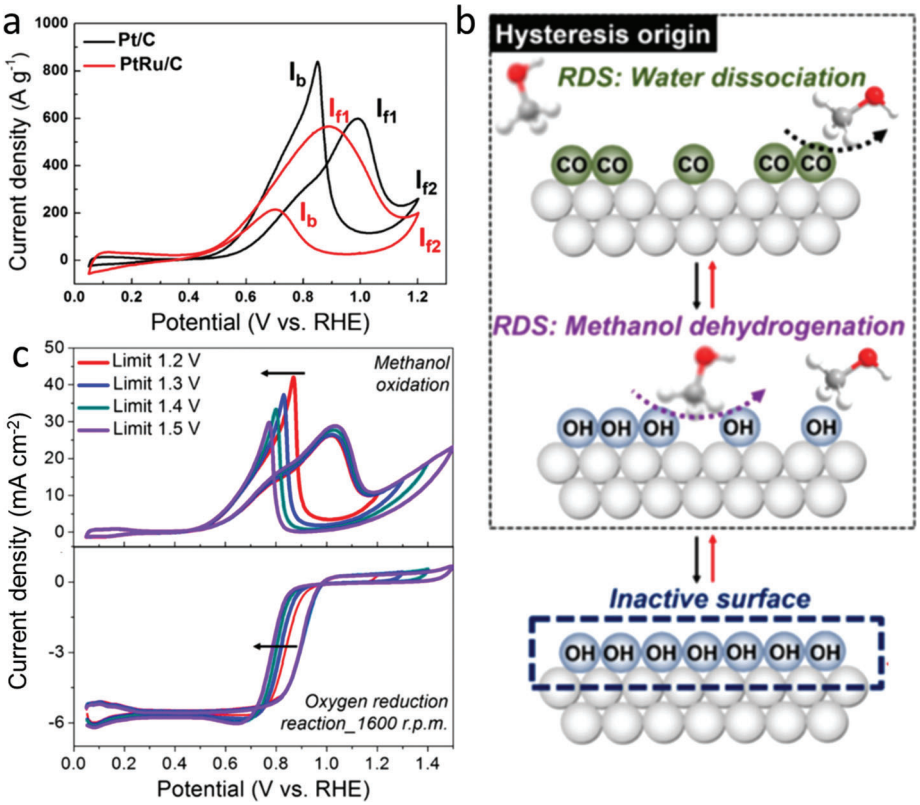

Figure 4. a) CV of MOR for Pt/C (black) and PtRu/C (red). b) Schematic illustration of the change of RDS for MOR at different potentials. c) MOR and ORR of Pt/C with different anodic limit potential. a–c) Reproduced with permission.[60] Copyright 2016, American Chemical Society.

in the forward and backward scan (I_f/I_b) has been intensively used to evaluate the CO anti-poisoning capability of MOR electrocatalysts. The origin of this criterion should trace back to an early study of MOR reported by Goodenough's group in 1992.[64] They contributed the I_f to the oxidation of freshly chemisorbed methanol while I_b was suggested to the oxidation of residual intermediates. Following this research, Liu and coworkers proposed that the ratio of I_f/I_b could be used as an important criterion to estimate the degree of CO tolerance of electrocatalysts.[65] Under this interpretation, a high ratio means a sufficient methanol electrooxidation process during the forward scan with fewer carbonaceous residues left. Further, they suggested the high I_f/I_b peak ratio of PtRu electrocatalysts is associated with their high efficiency toward methanol electrolysis. Till recently, this criterion is still adopted and used in many studies.

However, the current ratio criterion has been questioned by many other researchers. Tong et al. proposed an opposite conclusion for the first time based on in situ FTIR that both the I_f and I_b comes from the oxidation of methanol,[66] because the CO* signals on Pt/C and PtRu/C electrocatalysts all disappeared at above 0.8 V (vs Ag/AgCl). Furthermore, Sung and coworkers presented more detailed investigations to debate the origin of I_f/I_b via the study of CV and electrochemical impedance spectroscopy.[60] They stated that the changed RDS in the forward and backward scans resulted in peak hysteresis (Figure 4b). In detail, from 0.4 to 0.5 V (vs RHE), the Pt surface is totally covered with CO* which inhibits the progress of the reaction. In the next region (0.6–0.75 V), the slow reaction between CO and OH becomes the RDS. Following that, with the enhancement of the reaction kinetics for intermediates oxidation, the RDS turns into the oxidation of methanol to intermediates. However, with the potential increases further, the coverage of extra OH would block the available active sites on the Pt surface for methanol adsorption and results in a decreased current density. In the back scan process, the Pt surface is almost completely covered by OH, and thereby the methanol dehydrogenation is the RDS. With the increase of anodic limit potential, the oxidized Pt surface is harder to be reduced, leading to negatively shifted backward scan curves, and this trend is consistent with the case of ORR (Figure 4c). After all, the authors concluded that a higher I_b for Pt compared to PtRu is due to its easier OH reduction nature and the value of I_f/I_b does not represent the CO anti-poisoning capability but the degree of oxophilicity of electrocatalysts. This viewpoint has been supported by many other researchers.[67–69] Therefore, unless new evidence can be provided to further prove the relevance of I_f/I_b to the anti-poisoning capability of electrocatalysts, this criterion is not suggested to be used anymore. Instead, the CO-stripping test is reasonable to assess the anti-CO poisoning ability of the electrocatalysts.[70]

3.2. CV for Stability Test

After long-term electrolysis, electrocatalysts may suffer from irreversible structural damage (aggregation or Oswald ripening process), slow dissolution, significant surface reconstruction, and

poisoning, which can lead to performance degradation. Therefore, catalyst durability is a critical parameter that needs to be considered for practical applications.[71] While, the catalyst stability in the three-electrode system is usually characterized via the CA, chronopotentiometry, or CV test with desired operating conditions for at least hours. In most cases, all of these three tests can refer to the stability after a long-term operation and the catalytic activity degradation often cannot be restored.

However, MOR catalysts, basically the Pt- or Pd-based catalysts, are very prone to be poisoned by the intermediates such as CO during the methanol oxidation process. The strongly adsorbed carbonaceous species usually block the active sites and cause a fast decay of the catalytic performance. For MOR, this specific reaction, the CV test seems to be much more stable than the CA test: most of the reported catalysts suffer more than 70% current drop within 1 h during the CA test while they can perform more than hundreds of CV cycles without obvious decay.[50,72–75] This is because the toxic species can be removed in a high-potential region during the CV scan but will accumulate during the CA test. The DMFCs are operated at a certain potential in practical use, therefore, we would like to emphasize that the CA test is more reasonable to evaluate the long-term durability of the MOR electrocatalysts.

Notably, monitoring the evolution of the electrocatalysts during the electrochemical tests is also important. Newly developed in situ/operando characterization methodologies including electrochemical liquid cell transmission electron microscopy (TEM) and X-ray absorption spectroscopy are powerful tools to provide morphology, composition, valence state, and chemical bonding information during the reaction process.[76] Besides the complete oxidation product of CO_2, a significant amount of byproducts like HCOOH, HCHO, and $HCOOCH_3$ are also produced, which highlights the importance of assessing the catalyst selectivity. Furthermore, qualitative analysis of the reaction intermediates and products from methanol oxidation, which is usually ignored in most studies, is crucial for the validity of the catalyst benchmarking, the proposed mechanism, and the conducted theoretical studies. It is of necessity to combine different techniques like ATR-SEIRAS, in situ Raman spectroscopy, online DEMS, NMR spectroscopy, and high-performance liquid chromatography for accurate detection of different kinds of species involved in the reaction (like adsorbed surface species, dissolvable, and volatile products).[76–78]

In practical DMFCs, the operation conditions are very different compared with the lab-scale test, and more factors can affect the performance of catalysts. Previous studies demonstrated that the MA values of catalysts at the MEA level could decrease by one order of magnitude compared with the values measured by the lab three-electrode system.[79] In addition, the shape geometries of nanostructured catalysts may suffer great damage in practical applications.[80] Therefore, it is urgent to build new criteria to link the lab-scale research and the practical DMFC applications.

4. Advanced Electrocatalysts for MOR: From Nanosized Catalysts to SACs

The MOR is a complex six-electron transfer process, which involves multiple steps and many carbon-containing intermediates with the final product of CO_2. The catalysts for MOR should follow the rules that enable to adsorb methanol, favor the scission of the C–H/O–H bond, and speed up the conversion from carbonaceous intermediates to CO_2. It should be noted that if an active site is highly active toward methanol dissociation, it is usually unable to access the CO oxidation at low potentials. In this respect, increasing the multifunctionality of electrocatalysts has been recognized as the key strategy to breaking the scaling relationship of single-component catalysts. In this part, recent progress of advanced nanosized and single-atom MOR electrocatalysts will be summarized with emphasis on the fundamental design science (**Figure 5**).

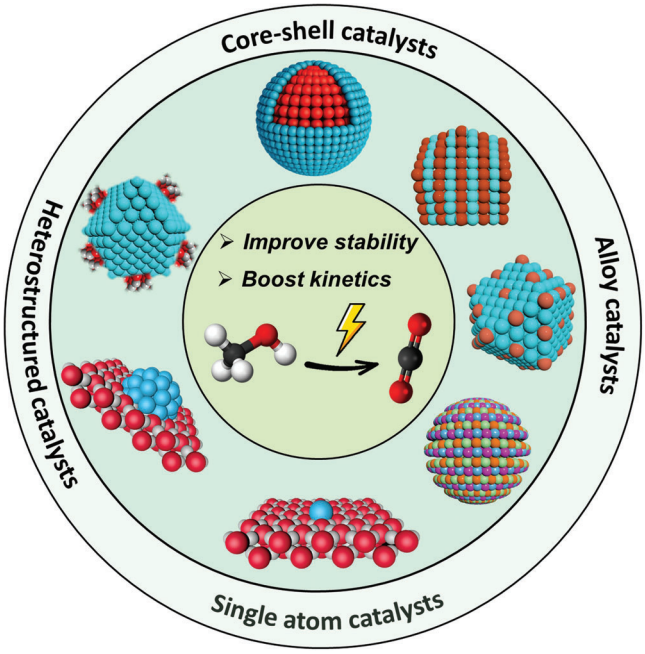

Figure 5. Advanced electrocatalysts toward the MOR.

4.1. Emerging Alloy Catalysts

Alloying Pt/Pd with one or more of the oxophilic elements such as Ru,[81–85] Ni,[83,86–88] Co,[86,88–90] Cu,[84,91–93] Fe,[94–96] and Ag[97–99] is the most traditional method to improve their MOR activity. A great challenge for the alloy system is that the introduced metals may dissolve into the reaction solution during the electrocatalysis process. Many studies suggest that the ordered intermetallic catalysts show higher catalytic activity and durability than their disordered phases.[100–103] Compared with random alloyed and ordered intermetallic catalysts which have been discussed in many previous reviews,[104–107] high-entropy alloys (HEAs) and single-atom alloys (SAAs) are two new emerging alloy systems and have attracted intense research interests toward methanol electrocatalysis.

4.1.1. HEAs

HEAs are alloys consisting of five or more elements in high concentrations (5–35 at%) and have many superior advantages, such

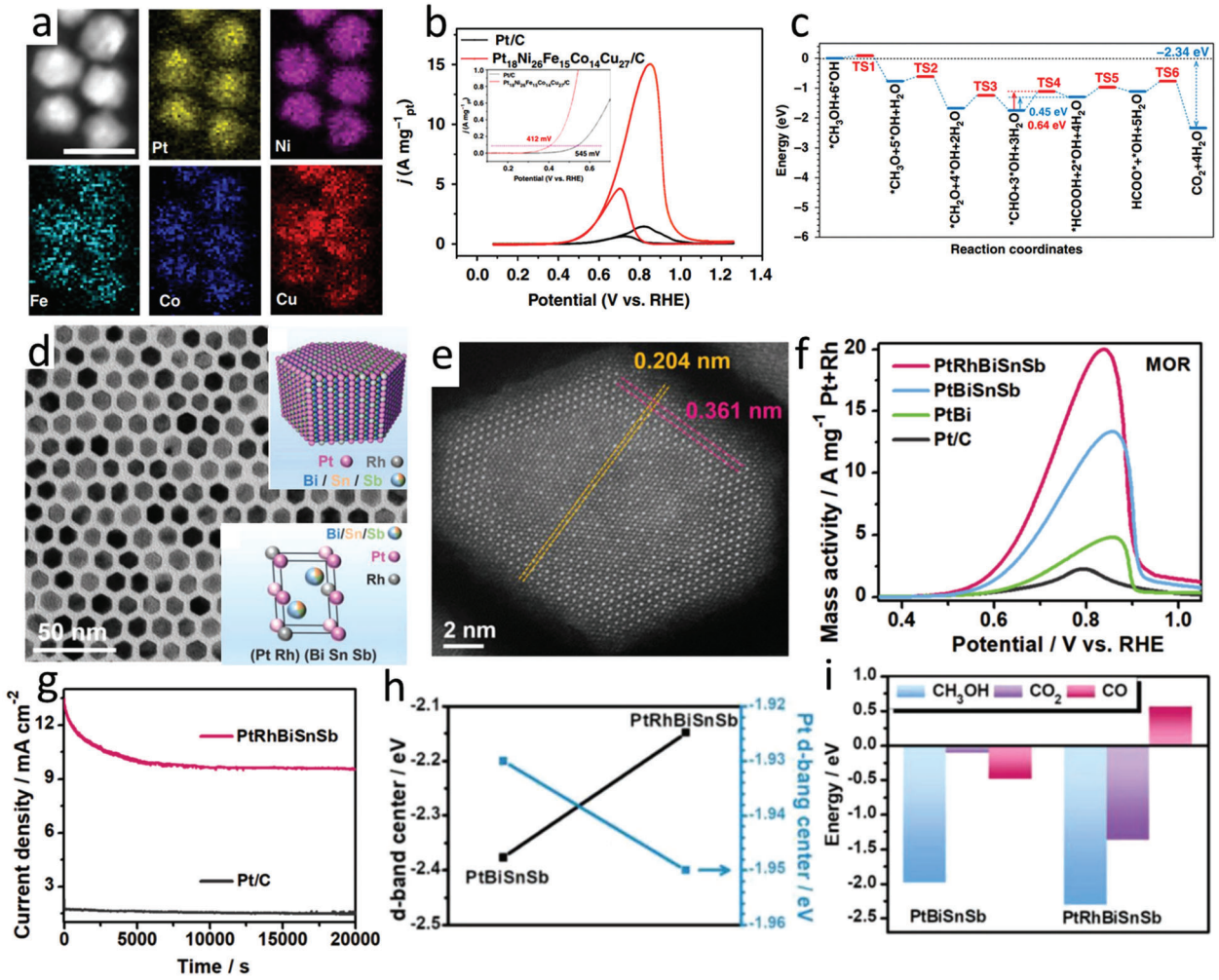

Figure 6. a) The images of elemental mapping toward $Pt_{18}Ni_{26}Fe_{15}Co_{14}Cu_{27}$ NPs (scale bar = 5 nm). b) CV curves of Pt/C and $Pt_{18}Ni_{26}Fe_{15}Co_{14}Cu_{27}$/C in 1 M KOH with 1 M CH_3OH electrolyte. c) The calculated energetic pathway of the MOR steps. a–c) Reproduced with permission.[111] Copyright 2020, Springer Nature. d) TEM image, the atomic arrangement and structural models (insets of (d)), and e) aberration-corrected HAADF-STEM image of PtRhBiSnSb HEI nanoplates. f) CV curves and g) long-term CA tests for different catalysts in 1 M KOH with 1 M methanol. h) The electronic structure and i) adsorption energy for methanol, CO_2, and CO for PtBiSnSb and PtRhBiSnSb nanoplates. d–i) Reproduced with permission.[112] Copyright 2022, Wiley-VCH.

as robust corrosion resistance, abundant atomic interfaces, and high mechanical strength.[108–110] Wang's group successfully synthesized $Pt_{18}Ni_{26}Fe_{15}Co_{14}Cu_{27}$ nanoparticles (NPs) with a size of around 3.4 nm via a one-pot oil phase synthesis method (**Figure 6**a).[111] Inspiringly, the as-prepared HEAs exhibit tenfold higher MA (15.04 A $mg^{-1}{}_{Pt}$) than that of commercial Pt/C (1.45 A $mg^{-1}{}_{Pt}$) and a much lower onset potential (Figure 6b). DFT calculations display that the 3d orbitals of Ni and Co elements serve as electron depletion centers during the MOR process. Meanwhile, the Cu-3d, Co-3d, and Fe-3d orbitals alleviate the reaction barrier and facilitate the stabilization of methanol oxidation intermediates. Furthermore, it can be observed from Figure 6c that, compared with CO-pathway, the MOR process prefers a CO-free pathway on the HEAs active sites which greatly suppresses the CO poisoning.

The hcp PtRhBiSnSb HEI nanoplates synthesized by Chen et al. also exhibited robust MOR performance.[112] Figure 6d shows the hexagonal nanoplates with an average edge length of around 6.2 nm. The atomic arrangement and crystalline unit models of the HEI nanoplates (insets of Figure 6d) illustrate that the as-prepared catalysts are ordered hcp quinary nanoplates with Rh atoms inserted into Pt columns and Sn/Sb atoms inserted into Bi columns. The high-angle annular dark-field scanning TEM (HAADF-STEM) image shows that the lattice spacing (0.361 nm) on the edge of nanoplates is located between that of (100) planes in the intermetallics of PtBi, PtSn, and PtSb (Figure 6e). The consistent lattice spacing of 0.204 nm ensures the identical hcp crystal structure of the nanoplate. The MOR performance in Figure 6f shows that the HEI nanoplates achieve a record-high MA of 19.529 A $mg^{-1}{}_{Pt+Rh}$, 8.6 times higher than that of Pt/C and obviously higher than that of PtBiSnSb and PtBi catalysts. Moreover, in the long-term CA test (20 000 s) for MOR at 0.7 V (vs RHE), the as-obtained PtRhBiSnSb HEI nanoplates exhibit a much higher current density compared with Pt/C, indicating their excellent durability (Figure 6g). DFT calculations prove that after the introduction of Rh, the overall d-band center

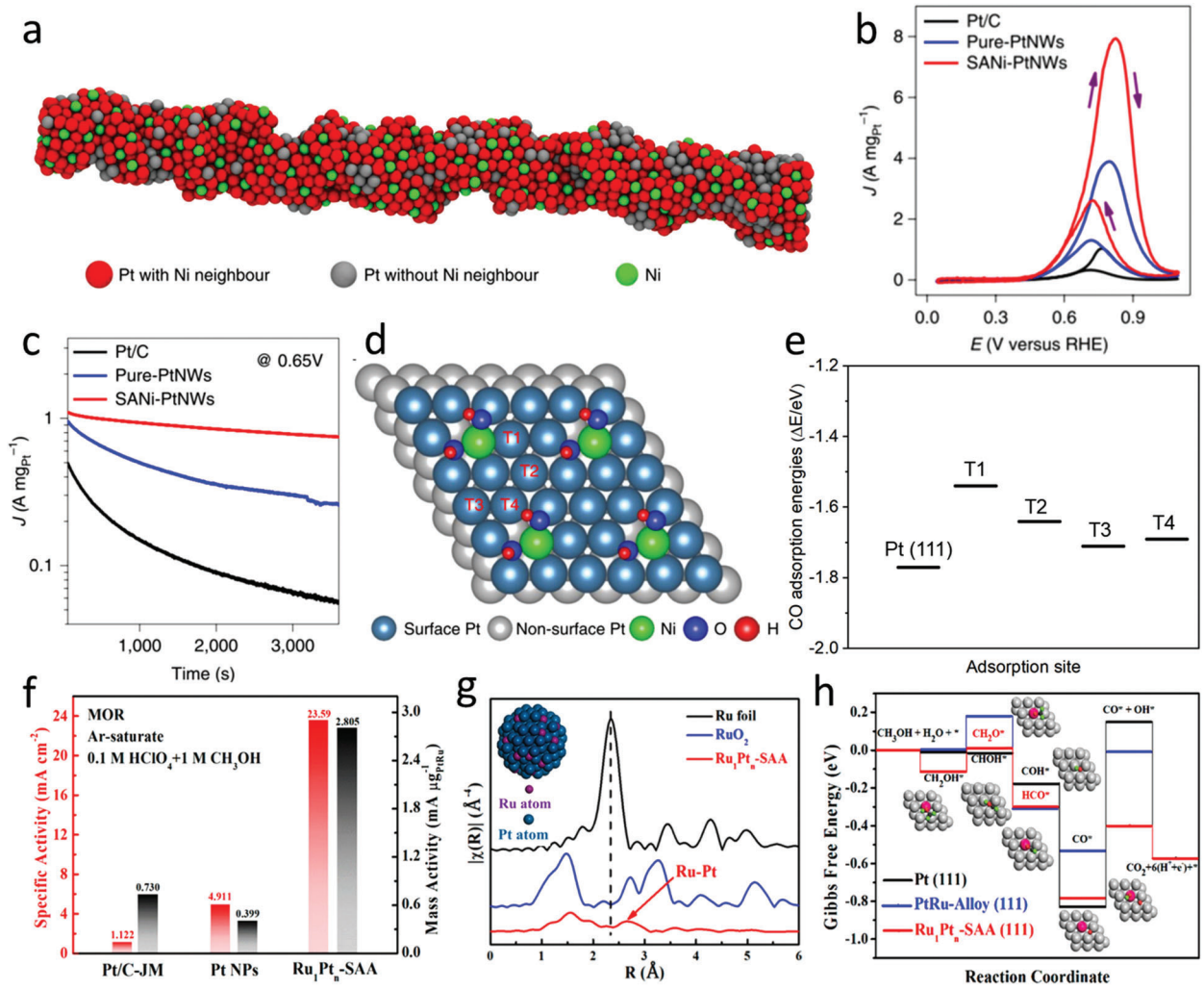

Figure 7. a) Schematic diagram of SANi-PtNWs. b) CV curves were tested in 1 M KOH and 1 M methanol. c) CA MOR test at 0.65 V vs RHE. d) Model illustration of the different CO adsorption sites (T1, T2, T3, and T4) on the SANi-PtNWs surface. e) CO adsorption energies on different sites. a–d) Reproduced with permission.[115] Copyright 2019, Springer Nature. (e) is plotted based on data obtained from ref. [115]. f) SA and MA of Ru_1Pt_n-SAA, Pt NPs, and Pt/C-JM. g) Ru K-edge EXAFS spectra of Ru_1Pt_n-SAA, RuO_2, and Ru foil. h) Calculated optimal MOR pathways on Pt (111), PtRu-alloy (111), and Ru_1Pt_n-SAA (111). f–h) Reproduced with permission.[116] Copyright 2022, American Chemical Society.

of PtRhBiSnSb has distinctly increased to improve its electron transfer efficiency. In contrast, the d-band center of surface Pt sites slightly decreased, suppressing the over-binding of the intermediates to guarantee efficient electrocatalysis (Figure 6h). Additionally, the strengthened adsorption of CH_3OH and CO_2, and unpreferred adsorption of CO on PtRhBiSnSb HEI nanoplates guarantees a CO-free pathway during the MOR process, leading to a much-improved catalytic durability (Figure 6i).

To conclude, HEAs enable multiple active sites which enhance the chance to properly tune the adsorption energy of key intermediates toward multi-electron-involving MOR. However, the almost infinite possible combinations of elements make it hard to dig out the real structure–activity relationship. The application of HEAs as active electrocatalysts in MOR is by far very limited and the explanation for the function of each element toward the enhanced catalytic behavior is hard to be thoroughly explored.[113,114]

4.1.2. SAAs

SAAs have isolated metal atoms dispersed in another metal, which will ensure the smallest number of surface active sites be blocked when the isolated metal atoms serve as co-catalysts. Li et al. engineered single Ni atoms on Pt nanowires (SANi-PtNWs) by partial electrochemical dealloying PtNi alloy NWs (**Figure 7**a).[115] Seven times higher MA (7.93 ± 0.45 A mg$^{-1}{}_{pt}$) and 144 mV decreased overpotential were obtained for SANi-PtNWs compared with commercial Pt/C (Figure 7b). Impressively, compared to the rapid current decay of Pt/C during a 3600 s CA test, the SANi-PtNWs show a quite stable catalytic performance (Figure 7c). Figure 7d shows SANi-PtNWs have four different adsorption sites for CO (labeled as T1, T2, T3, and T4). Moreover, all of the adsorption sites on the SANi-PtNWs surface show a weaker COBE than that of Pt/C, facilitating the final step conversion from CO to CO_2 (Figure 7e). The

Ru_1Pt_n SAA (single Ru atoms dispersed in Pt nanocrystals) developed by Liang's group also exhibited superior MOR activity with a high SA of 23.59 mA cm^{-2} and MA of 2.805 mA μg^{-1}_{PtRu} which is 21.0 and 3.84 times higher than that of Pt/C, respectively (Figure 7f).[116] The absence of Ru−Ru scattering in the Fourier transformed-extended X-ray absorption fine structure (FT-EXAFS) curves of Ru K-edge indicates that Ru is atomically dispersed in Pt nanocrystals (Figure 7g). XAFS, X-ray photoelectron spectroscopy (XPS), as well as the DFT results show that electrons transferred from Ru atoms to Pt atoms in Ru_1Pt_n-SAA. Therefore, the elevated Fermi level of Pt atoms results in a decreased COBE and the lowered Fermi level of Ru atoms leads to an increased OHBE, which greatly enhanced the MOR kinetics of Ru_1Pt_n-SAA (Figure 7h). Recently, Kong and co-workers have successfully deposited atomic Ru on the surface concavities of PtNi NPs.[63] The obviously upshifted d-band center induced by Ru single atoms causes an increased OHBE which boosts the removal of CO* and results in a high MA activity of 2.01 A mg^{-1}_{Pt}. The above studies have shown that single-atom promoter enables effective regulation of the d-band center of their adjacent sites. Therefore, SAAs have significant potential in accelerating the MOR kinetics with the minimum blocking of surface active sites and deserve specific research attention in the future.

4.2. Core–Shell Catalysts

Precisely regulating the strain effect is important but difficult to be achieved in alloy systems. In this regard, the core–shell structure is an efficient model to study the strain effect on MOR performance, because the strain can be accurately modulated by controlling the thickness of the shell or changing the nature of the core.[117,118] The modification of core–shell catalysts can alter the electronic structure through tuning the lattice strain at the heterointerface.[119,120] The changed electronic structure would modulate the interaction with adsorbates which can be interpreted by the d-band theory.[119,121,122] As illustrated in **Figure 8**a, increased atom distance will result in a tensile strain and an upward-shifted d-band center. Meanwhile, the antibonding states will be less filled, causing a stronger interaction between the adsorbates and the catalysts. In contrast, compressive strain decreases atomic distance and pushes the d-band center downward, leading to a weaker adsorbate–catalyst interaction.

Considering the strong CO adsorption on Pt/Pd is one of the key problems for MOR, compressive lattice strain was usually considered to accelerate the sluggish reaction by pushing the d-band center downward, allowing a weaker CO adsorption.[100,123,124] On the other hand, it has also been reported that the tensile strain effect can be beneficial to activity enhancement.[12,125–127] For example, in the Pt_3Ga intermetallic nanocrystals with two-to-three atomic-layer Pt on the surface (AL-Pt/Pt_3Ga),[56] the formed tensile strain makes all the intermediates (CO* + OH*) binding more strongly for easily activating water and removing CO*. The Au@PdPt core–shell catalysts prepared by Yang et al. also exhibit a significantly improved MOR performance compared with Pt/C.[12] The enhanced catalytic behaviors were attributed to the strengthened adsorption of $*CH_3OH$ and the lowered reaction barriers induced by tensile strain.

Although core–shell catalysts have been developed for many years, it is important to map in detail the strain–activity correlations toward the MOR.[128] To this end, Jin et al. recently deposited ultrathin Pt shells on Pd-based nanocubes. A strain change ranging from −5.1% to 5.9% can be obtained via a phosphorization and dephosphorization process (Figure 8b,c). They found that the electrocatalytic activity of the Pt shells follows an M-shaped curve with continuous strain changes (Figure 8d,e). DFT calculations give further insight into above observations. The increased tensile strain strengthens the OHBE, benefiting the removal of CO* to some degree, but too much tensile strain would also result in strongly adsorbed CO*. Whereas, the opposite effect occurs with compressive strain. The strong compressive strain not only weakens CO* binding (Figure 8j) but also weakens the OH* adsorption (Figure 8f) making it difficult to oxidize CO*. Therefore, the authors proved that only moderate lattice strains, either tensile smaller than 4.7% or compressive smaller than 3.9%, promote the MOR catalytic activity of Pt via boosting CO removal. This approach has a great significance in strain-engineering enhanced electrocatalytic performances.

4.3. Heterostructured Catalysts

Heterostructured catalysts with abundant interface enable boosted MOR kinetics via the synergistic effect from different components. Moreover, electron transfer and charge redistribution also commonly exist in the interface of heterostructured catalysts which can tune the electronic structures of active sites and further modulate their adsorption energies with adsorbates.[129,130]

4.3.1. Heterostructured Catalysts with Functional Substrates

Placing Pt/Pd units on the oxophilic substrates is a well-studied system. A typical example is the Pt–$Ni(OH)_2$–graphene electrocatalysts designed by Huang et al.[50] The highly defective $Ni(OH)_2$ nanostructures adjacent to Pt sites are believed to speed up the oxidation of carbonaceous poison species via promoting the adsorption of OH*. Many other heterostructured electrocatalysts such as Pt–$Ce(CO_3)OH$/reduced-graphene-oxide (rGO) electrocatalyst,[131] Pt/MnO_2/graphene,[132] Pt/Mn_3O_4/rGO,[133] Pd–V_2O_5/C,[134] Pd/Co–CeO_2,[135] Pd–PdO porous nanotubes,[73] and Pd–Mn_3O_4/MWCNT[136] were also prepared based on the similar mechanism. Apart from the bifunctional mechanism, the interface between supported metals with metal oxide substrates may also exist electron transfer.[15] For example, Wang's group prepared the oxygen vacancies-rich CeO_2 nanorods via plasma etch.[137] The defective CeO_2 affords surplus electrons to the loaded Pt NPs and reduces its chemisorption with CO* which is beneficial for MOR.

Graphene and its carbon derivatives are the most frequently used supports for anchoring active catalysts. It has been reported that heteroatom with low electronegativity like B-doped (2.0)[138,139] and P-doped (2.1)[140,141] carbon materials can increase the electron density of Pt/Pd and lower their d-band center. Therefore, the lowered adsorption energy of CO* will benefit the MOR kinetics at low potentials. In addition, the heteroatom-doped carbon itself can also assist the MOR. For example,

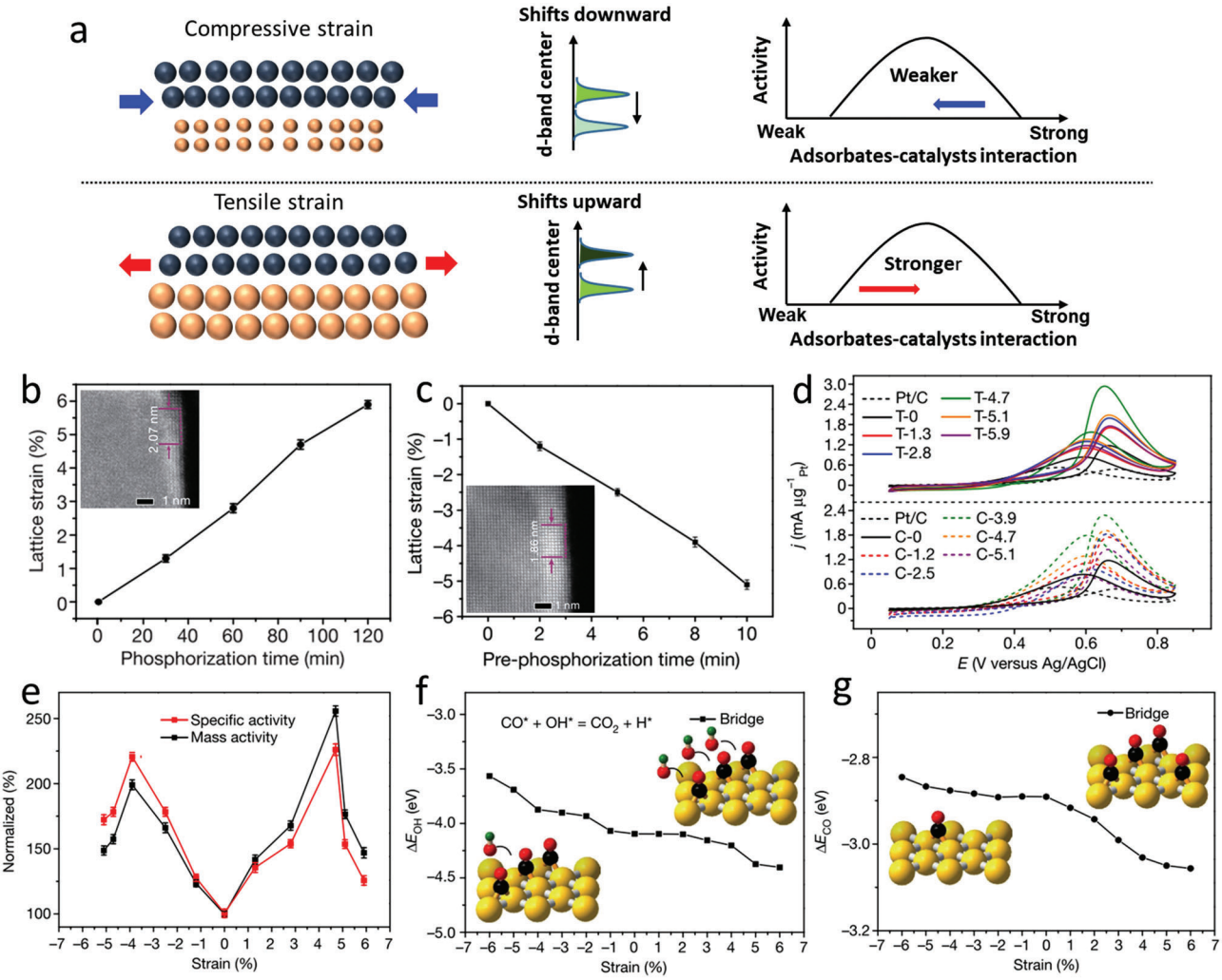

Figure 8. a) Illustration of the strain effect on the change of d-band center and adsorbates–catalysts interactions. b,c) Profiles describing the increasing Pt lattice tensions (b) and the increasing Pt lattice compressions (c) induced by phosphorization and dephosphorization process. d) CV curves of different strained Pt shells catalysts in 0.5 M H_2SO_4 and 1 M CH_3OH. e) Normalized MOR catalytic activities shown in (d). f,g) Adsorption energies of OH* (f) and CO* (g) at bridge sites and strain-related atomic models. b–g) Reproduced with permission.[128] Copyright 2021, Springer Nature.

N atoms with larger electron affinity could provide abundant OH sources to oxidize CO.[139,142] Besides the abovementioned traditional supports, intensive efforts have been devoted to engineering supports for increasing the interface complexity.

Recently, our group introduced single Co atoms to functionalize the N-doped carbon nanosheets (Co–N–C).[143] Pt NPs with an average size of around 3.0 nm were then loaded on Co–N–C substrate via ethylene glycol reduction. The introduction of Co single atoms caused a decreased electron density of Pt NPs. In this case, though the upshift of the d-band center of Co–N–C/Pt increased its adsorption with CO*, the stronger interaction of OH* facilitates the desorption of CO* and results in a greatly promoted MOR performance (**Figure 9**a). In all, the incorporated Co single atoms not only optimize the electronic structure of adjacent Pt NPs but also boost the adsorption of OH* on Co sites, assisting the removal of CO* accordingly (Figure 9b). Graphdiyne (GDY) with sp and sp^2 hybrid electronic structure and good electron/proton conductivity, has triggered intensive research interests since its first investigation in 2010.[144] Recently, GDY has also been used in the MOR catalyst system.[145,146] Li and coworkers anchored $Pt_{4.4}Cu$ NPs into the GDY nanochannel as illustrated in Figure 9c.[145] The superior protophilic ability of GDY favors the proton migration during MOR which not only reduces the energy barriers in each reaction step but also leaves more active sites for the reaction proceeding (Figure 9d). It can be observed in Figure 9e that in the DMFC system, the power densities of GDY@PtCu surpass commercial PtRu/C at all the tested temperatures.

MXenes as a new member of 2D materials, feature good conductivity and rich functional groups and have attracted intense research interests as promising support materials.[147] Zhu et al. synthesized 3D $Ti_3C_2T_x$ MXene balls supported Pt clusters ($Ptc/Ti_3C_2T_x$) by a spray-drying method.[148] It can be seen from the HAADF-STEM image (Figure 9f) that the size of Ptc is around 1.5 nm and evenly distributed on the substrate. The DFT calculation demonstrates that 2.17 electrons transfer from the Ptc to

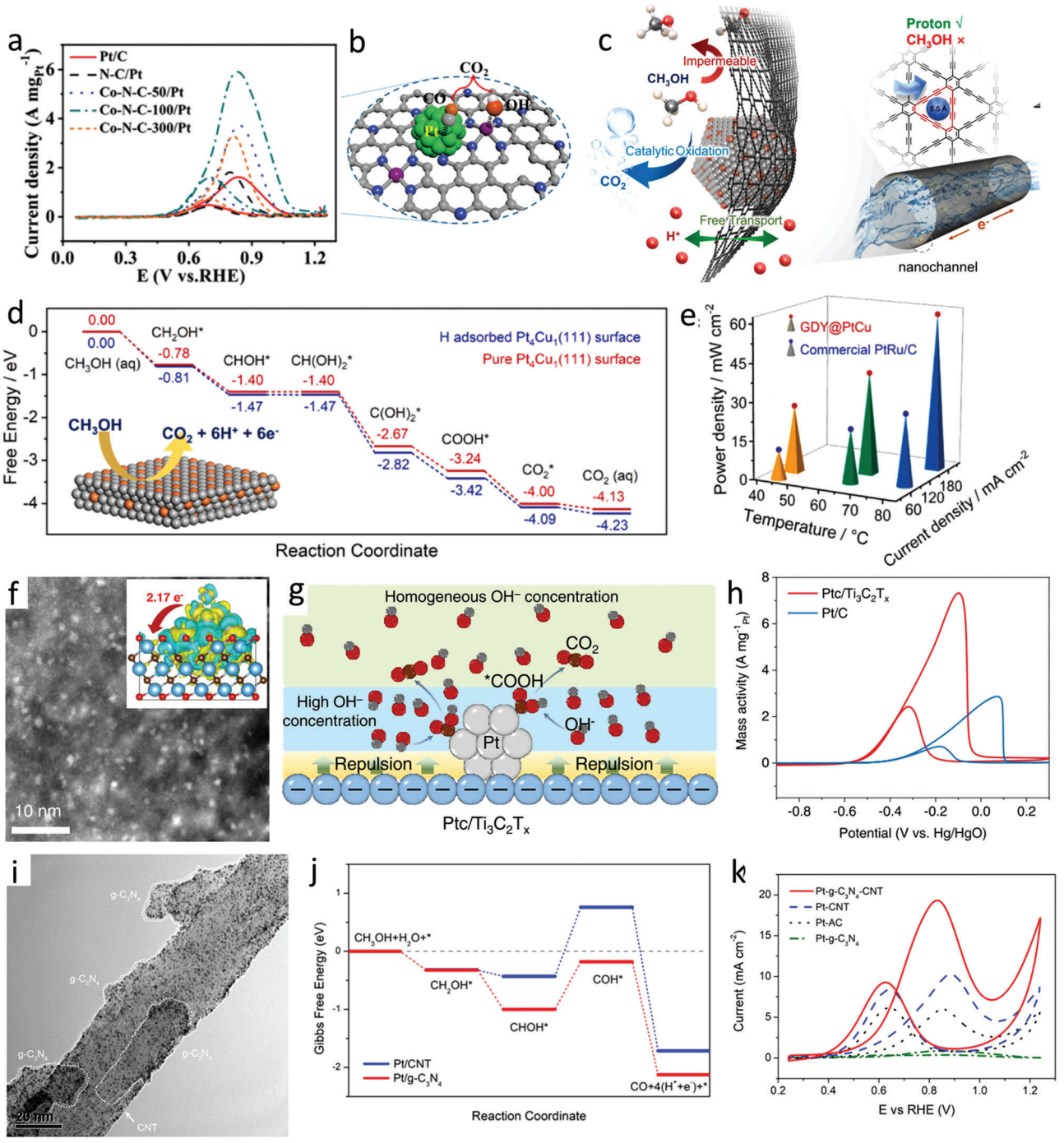

Figure 9. a) CV curves of Pt/C and Co–N–C/Pt with different amount of Co atoms in 3.0 M methanol with 1.0 M KOH. b) Scheme illustration of the promotion mechanism of Co–N–C/Pt catalysts. a,b) Reproduced with permission.[143] Copyright 2022, Wiley-VCH. c) Schematic illustration of GDY@PtCu. d) Free energy diagrams of MOR on the Pt_4Cu (111) surface with and without the presence of H*. e) The power density for the GDY@PtCu and the PtRu/C conducted at 0.35 V with different temperatures. c–e) Reproduced with permission.[145] Copyright 2021, Elsevier. f) HAADF-STEM image of Ptc/$Ti_3C_2T_x$ and the inset shows the calculated charge density difference. g) Schematic illustration of the proposed MOR mechanism on Ptc/$Ti_3C_2T_x$. h) CV of Pt/C and Ptc/$Ti_3C_2T_x$ in 1.0 M methanol with 1.0 M KOH. f–h) Reproduced with permission.[148] Copyright 2022, American Chemical Society. i) TEM image of Pt–g-C_3N_4–CNT. j) Calculated reaction free energy for the MOR on Pt/CNT and Pt–g-C_3N_4. k) CV curves tested in 0.5 M H_2SO_4 with 1.0 M methanol solution. i–k) Reproduced with permission.[154] Copyright 2019, American Chemical Society.

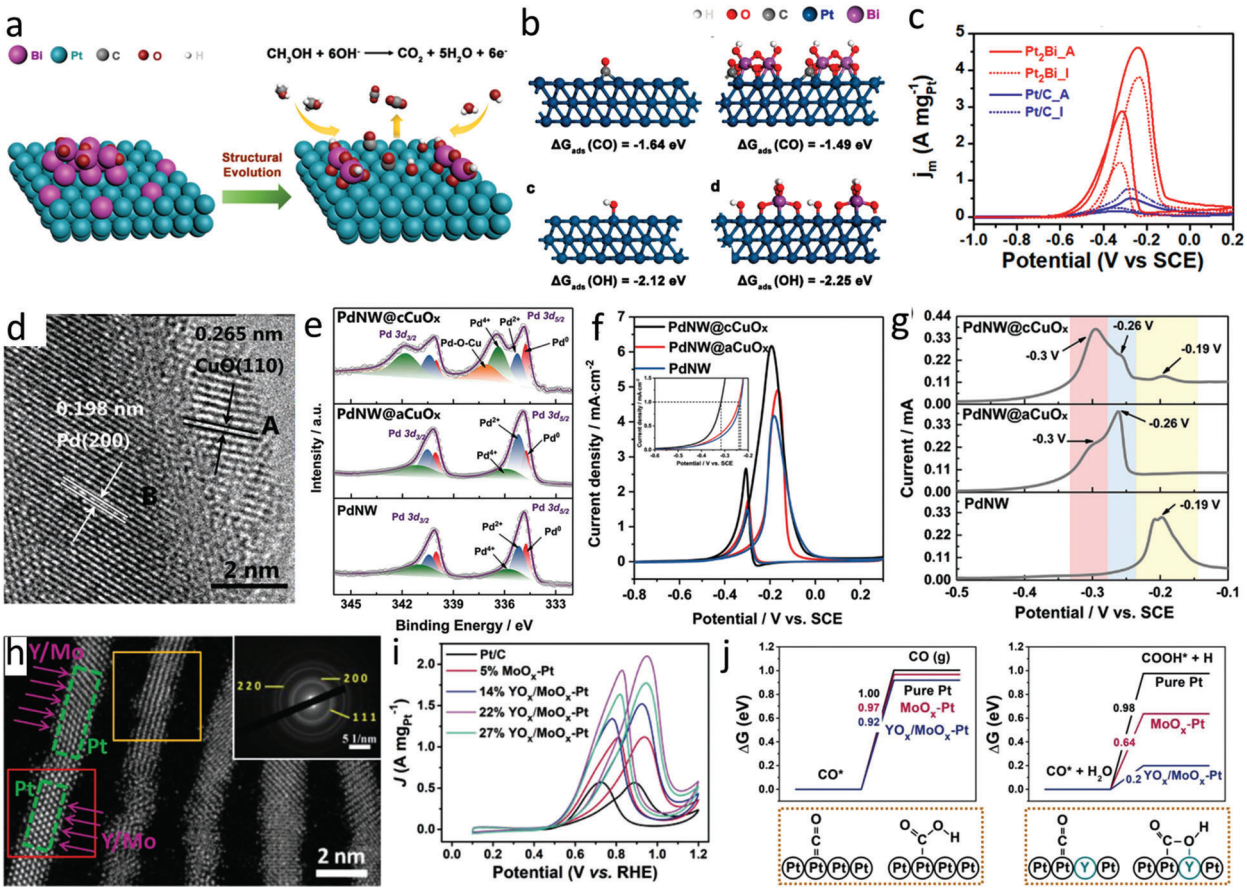

Figure 10. a) Schematic illustration of the preparation of $BiO_x(OH)_y$–Pt inverse interface via electrochemical reconstruction for boosted MOR. b) DFT calculation of the COBE and OHBE on the surfaces of Pt (111) with and without $BiO_x(OH)_y$ decoration. c) CV curves of Pt/C and Pt_2Bi before (_I) and after (_A) electrochemical treatment in 1.0 M KOH with 1.0 M methanol. a–c) Reproduced with permission.[160] Copyright 2020, American Chemical Society. d) HRTEM image of PdNW@cCuO$_x$. e) High-resolution elemental XPS spectra of Pd 3d and Cu 2p for different catalysts. f) MOR CV curves and g) CO-stripping voltammograms in 1.0 M KOH with and without 1.0 M methanol, respectively. d–g) Reproduced with permission.[161] Copyright 2019, Wiley-VCH. h) HAADF-STEM image and corresponding SAED pattern (inset) of 22% YO_x/MoO_x–Pt NWs. i) MOR CV curves tested in 0.1 M $HClO_4$ with 0.5 M methanol. j) Free desorption and oxidation energy changes of CO* on pure Pt, MoO_x–Pt, and YO_x/MoO_x–Pt surfaces; the corresponding adsorption strategies for CO* and COOH* on pure Pt and YO_x/MoO_x–Pt surfaces are shown below. h–j) Reproduced with permission.[72] Copyright 2021, Wiley-VCH.

the substrate, resulting in a positively charged Pt and negatively charged $Ti_3C_2T_x$ (inset of Figure 9f). The authors inferred that the introduced repulsion force between OH^- and electron-rich $Ti_3C_2T_x$ would provide a high local OH^- concentration around positively charged Ptc and enhance the removal of adsorbed CO* (Figure 9g). In all, with the assistance of $Ti_3C_2T_x$, the Ptc/$Ti_3C_2T_x$ exhibits a high MA of 7.32 A mg^{-1}_{Pt} which is nearly three times higher than that of Pt/C (Figure 9h). Zhou and co-workers also proved that the electronegative terminations of $Ti_3C_2T_x$ enable strong metal–support interactions which will optimize the electronic structure of loaded Pd and favor the adsorption and oxidation of methanol molecules.[149]

In addition, graphitic carbon nitride (g-C_3N_4) has high nitrogen content and good chemical and thermal stability, but its applications are greatly restricted by low conductivity. However, many reports have proved that the marriage of g-C_3N_4 with conductive carbon materials can serve as advanced substrates for accelerated MOR.[150–153] For example, Zhang et al. covalently coupled g-C_3N_4 with carbon nanotubes to support Pt clusters and the prepared hybrid has strong catalyst–support interactions (Figure 9i).[154] XPS and theoretical calculations identify that compared with Pt–CNT, the π-bonded planar g-C_3N_4 keeps the immobilized Pt with more metallic properties and makes it more energetically favorable in multi-step reaction pathways (Figure 9j). As a result, Pt–g-C_3N_4–CNT shows higher MOR activity and decent poison tolerance compared with Pt–CNT (Figure 9k).

4.3.2. Inverse Heterostructured Catalysts

Inverse heterogeneous nanostructures with oxides or other compounds decorated on the noble metal surface have attracted intensive research interests but have rarely been studied in MOR systems.[155–159] Zhang and co-workers designed a $BiO_x(OH)_y$–Pt inverse heterostructured electrocatalyst via electrochemical reconstruction (**Figure 10**a).[160] The electron redistribution at the heterostructure interface leads to a weakened CO adsorption and strengthened OH adsorption at the interface region (Figure 10b).

As a result, the obtained $BiO_x(OH)_y$–Pt electrocatalyst exhibits a superior MA which is 5.96 times higher than that of 20 wt% Pt/C (Figure 10c). The merged two components at the inverse heterostructure interface may result in the formation of new chemical bonds. Chen et al. successfully decorated the crystalline CuO_x layer on the Pd nanowire (PdNW@cCuO_x, Figure 10d).[161] XPS spectra (Figure 10e) show the existence of electron-deficient $Pd^{\delta+}$ species and rich Pd–O–Cu interfaces in PdNW@cCuO_x system. The detailed analysis reveals that the greatly enhanced MOR activity (Figure 10f) and stability of the PdNW@cCuO_x are ascribed to the strong Pd–O–Cu interaction and the weakened CO* bonding (Figure 10g). Moreover, the introduction of oxophilic metal species on the active metal may also alleviate the intermediate poisoning issue via a decoupling mechanism. For instance, Guo and co-workers decorated sub-monolayer YO_x/MoO_x on ultrathin platinum nanowires (YO_x/MoO_x–Pt NWs, Figure 10h).[72] It can be observed from Figure 10i that the 22% YO_x/MoO_x-decorated Pt NWs exhibit the best MOR performance with the SA of 3.35 mA cm^{-2} and MA of 2.10 A mg^{-1}_{Pt}, exceeding those of Pt/C by 2.21 and 3.75 times, respectively. The in situ FTIR spectroscopy shows that CO_2, the final product of MOR, appears at a much lower potential (0.40 V) for YO_x/MoO_x–Pt NWs than that of commercial Pt/C (0.60 V), indicating that the decoration of YO_x/MoO_x can induce the CO* thermodynamically transferred from linear mode (CO_L) to bridge mode (CO_B) and lower the barrier of its further oxidation. DFT calculations further evidence a decoupling mechanism to restricting the CO poisoning issue, where YO_x and MoO_x decoupled with CO* and COOH*, bringing in lowered free energy barriers for their oxidation reaction (Figure 10j). Above studies indicate that the rational fabrication of inverse heterostructured electrocatalysts can be a promising strategy for fabrication of high-performance MOR electrocatalysts.

4.4. SACs

SACs with single metal atoms functioning as the primary active sites have been applied in many electrocatalytic reactions,[162–165] however, they are believed to be inactive toward the MOR for a long time. It is well known that reducing the size of catalysts would increase the number of exposed active sites and lead to improved MOR performance.[166,167] However, the catalytic activity cannot always be enhanced by reducing the size of catalysts.[168] It has been proved experimentally that when the size is smaller than 4.5 nm, the specific MOR activity decreased with decreasing Pt particle size.[169] Additionally, 3–10 nm was found to be the optimum size range for Pt particles to obtain CO_2, and the particle smaller or larger than that size will result in partial oxidation products.[170]

In 2006, Cuesta modified Pt (111) electrodes with cyanide and obtained four possible kinds of reactive sites: 1) a single Pt atom, 2) two adjacent Pt atoms, 3) three Pt atoms arranged linearly, and 4) three Pt atoms arranged forming a chevron with a 120° angle.[171] Because barely any CO can be detected during the MOR test, the author claimed that the minimum atomic ensemble for the oxidation of methanol to CO_2 needs three contiguous Pt atoms for the CO pathway and two adjacent Pt atoms for the CO-free pathway. This result has been proved by many other researchers that SACs consisting of Pt single atoms dispersed on carbon nanotubes,[172] carbon black,[173] and MXene[148] are all inactive toward the MOR.

However, in 2021, Ciucci's group reported that atomically dispersed Pt atoms on RuO_2 (Pt_1/RuO_2, **Figure 11**a) are highly active toward the MOR with a MA of 6766 mA mg^{-1}_{Pt} which is almost 15.3 times higher than that of Pt/C.[173] Interestingly, one of the control samples, single Pt atoms on metallic Ru (Pt_1/RuO_2–H, prepared by reducing Pt_1/RuO_2 via H_2 at low temperature) shows no MOR activity (Figure 11c). The EXAFS spectra show a prominent peak at 1.62 and 2.49 Å for Pt_1/RuO_2 and Pt_1/RuO_2–H, which corresponds to Pt–O and Pt–Ru coordination, respectively (Figure 11b). In addition, XPS results also show that the RuO_2 in Pt_1/RuO_2 has a new peak at 531.3 eV which can be attributed to the appearance of oxygen vacancies on the surface. DFT calculations reveal that in Pt_1/RuO_2, the CH_3OH molecules would preferentially adsorb on the coordinatively unsaturated Ru (Ru_{cus}) and the undercoordinated bridging O (O_{br}) makes the scission of the O–H bond spontaneously (Figure 11d). However, for the single Pt atom on carbon or metallic Ru, the weak adsorption of CH_3OH and higher energy barriers for the O–H and C–H bonds scission make Pt_1/VXC-72 and Pt_1/RuO_2–H inert toward the MOR (Figure 11e). In all, the authors claimed that the RuO_2 substrate turns Pt single atoms into MOR-active.

More recently, Poerwoprajitno et al. synthesized single Pt atoms on Ru NPs by annealing Pt-island/Ru NPs at 200 °C in 5% H_2/N_2.[75] During the annealing process, the Pt islands can thermodynamically spread on Ru surface and the spreading process is observed via in situ TEM (Figure 11f). The single-Pt-atom-on-Ru catalyst shows high catalytic activity for MOR with a MA of 1.58 A mg^{-1}_{Pt} which is around two times and five times greater than Pt-island-on-Ru catalyst and commercial PtRu, respectively (Figure 11g). Moreover, the single-Pt-atom-on-Ru catalyst also exhibits a high resilience to CO. The performed DFT calculations show that stronger adsorption of CH_3OH and weaker adsorption of CO leads to the superior MOR performance of the single-Pt-atom-on-Ru catalyst than Pt-island-on-Ru and PtRu catalysts (Figure 11h,i). The authors highlighted that the DFT calculation results were obtained under the modeling at 0.6 V (vs RHE) and the surfaces of the catalysts were covered fully with OH groups. However, the catalyst surface adsorption state is potential-dependent which greatly affects the DFT results. In addition, it has been reported that SACs may be reconstructed into cluster structures as true catalytic active sites and then return to the initial atomic dispersion under working conditions.[174,175] Though significant breakthroughs in the field of active Pt SACs toward the MOR have been achieved, more attention still needs to be paid to exploring the dynamic structure evolution of SACs under working conditions and conquering the limitations of DFT calculations.

5. Conclusions and Perspectives

Recent development and limitations of MOR regarding the mechanism, evaluation criteria, and advanced electrocatalysts are summarized in this review. The MOR performance of recently reported advanced electrocatalysts is listed in **Table 1**. Despite the extensive research on MOR, challenges still remain and hinder its practical implementation in DMFCs. To impetus the further

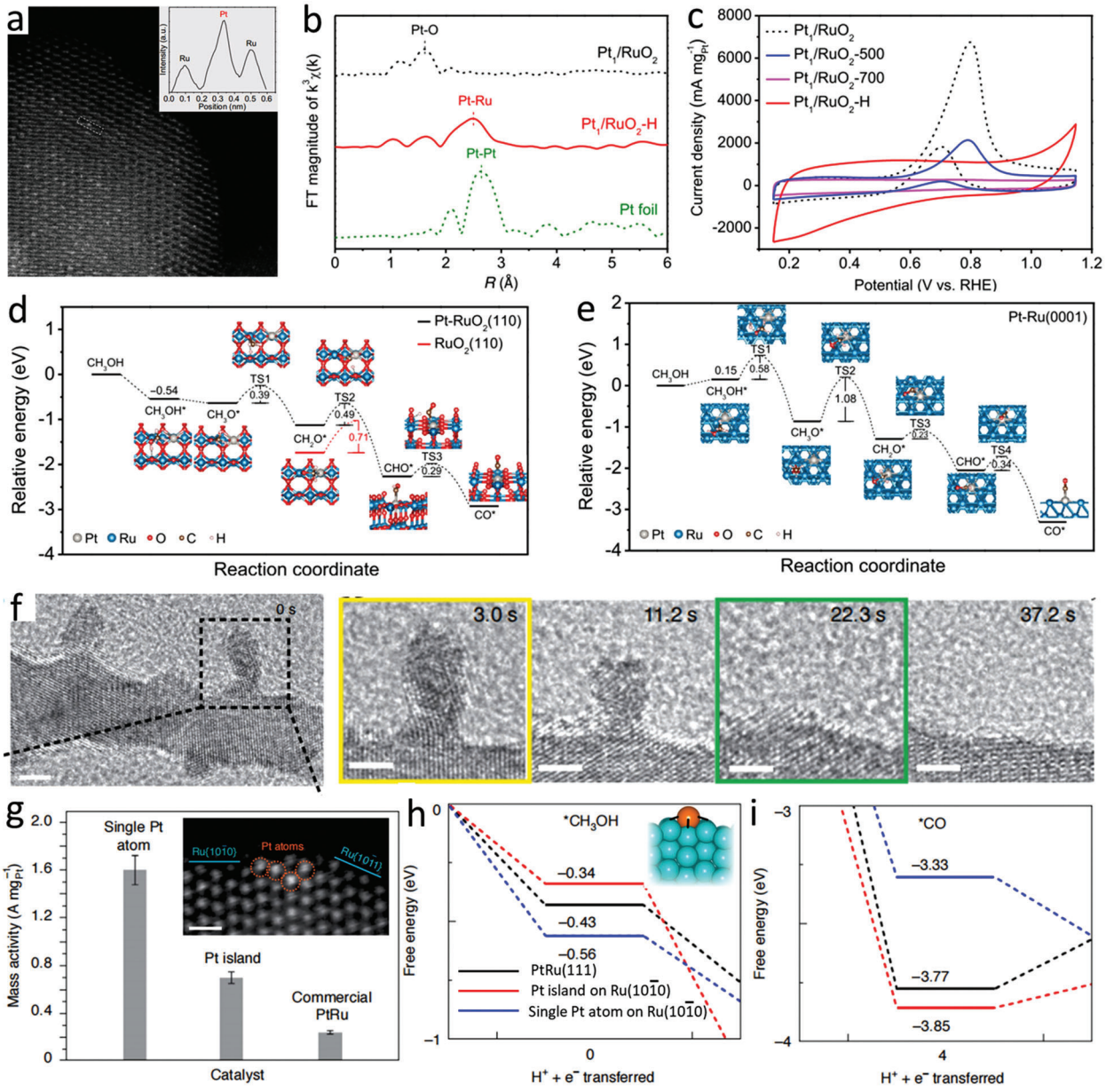

Figure 11. a) HAADF-STEM image of Pt_1/RuO_2; the inset shows the intensity profile along with the dashed rectangle. b) Ru k3-K edge EXAFS spectra of Pt_1/RuO_2, Pt_1/RuO_2–H, and Pt foil. c) CV curves collected in 0.1 M KOH with 1 M methanol. d,e) Free energy diagrams for methanol oxidation to CO at Pt-RuO_2 (110) and RuO_2 (110) (d), and PtRu (0001) (e). a–e) Reproduced with permission.[173] Copyright 2021, Springer Nature. f) HRTEM images of the evolution of Pt-island-on-Ru branch catalyst over time. Scale bar = 2.5 nm. g) MA of different catalysts. The inset shows an HAADF-STEM image demonstrating the position of Pt atoms in relation to Ru facets. Scale bar = 0.5 nm. h,i) Free-energy diagrams for adsorption of *CH_3OH (h) and *CO (i) on the active sites of different catalysts. The inset of (h) shows the calculated stable configuration of a single Pt atom on Ru (10$\bar{1}$0). f–i) Reproduced with permission.[75] Copyright 2022, Springer Nature.

developments of this field, we highlight that future research can be focused on the following aspects.

5.1. Strengthening the Understanding of the Mechanism for the MOR

For the methanol electrooxidation process, a two parallel paths mechanism is well accepted. The previous mechanism study was mainly based on platinum crystal electrodes; however, the evolution of the interaction between intermediates and active sites, the detailed competitive adsorption process, and even the RDS are poorly understood in polycrystalline and multimetallic systems. A deeper insight into the mechanism is crucial for the development of efficient MOR catalysts.

1) *Discovering the Adsorption Energy Scaling Relations*: An ideal electrocatalyst should have an optimal BE, neither too weak

Table 1. Summary of recently reported advanced electrocatalysts for the MOR.

Catalyst	Onset potential	MA [A mg^{-1}]	SA [mA cm^{-2}]	CA performance [Current loss]	Electrolyte	Reference
Au@PdPt	≈0.5	4.830	6.9	—	1.0 M CH_3OH + 1.0 M KOH	[12]
PtBi Nanorings	≈0.53	6.42	11.93	≈50% after 10 000 s	1.0 M CH_3OH + 1.0 M KOH	[13]
AL-Pt/Pt_3Ga	≈0.46	1.094	7.195	≈75% after 1000 s	1.0 M CH_3OH + 0.5 M H_2SO_4	[56]
YO_x/MoO_x–Pt NWs	≈0.5	2.10 A	3.35	≈60% after 3000 s	0.5 M CH_3OH + 0.1 M $HClO_4$	[72]
Pd–PdO nanotubes	≈0.6	1.1113	46.9	≈71.5% after 10 000 s	1.0 M CH_3OH + 1.0 M KOH	[73]
$Pt_{18}Ni_{26}Fe_{15}Co_{14}Cu_{27}$/C	≈0.41	15.04	—	≈14% after 5000 s	1.0 M CH_3OH + 1.0 M KOH	[111]
PtRhBiSnSb nanoplates	≈0.5	19.529	—	≈28% after 20 000 s	1.0 M CH_3OH + 1.0 M KOH	[112]
SANi-PtNWs	≈0.45	7.93 ± 0.45	—	≈31% after 3600 s	1.0 M CH_3OH + 1.0 M KOH	[115]
Ru_1Pt_n-SAA	≈0.5	2.805	23.59	≈80% after 5000 s	1.0 M CH_3OH + 0.1 M $HClO_4$	[116]
Ru-ca-PtNi	≈0.55	2.01	≈5	≈77% after 1000 s	0.5 M CH_3OH + 0.1 M $HClO_4$	[45]
Pt/CeO_2–P	≈0.5	0.714	8.06	≈75% after 5000 s	1.0 M CH_3OH + 0.5 M H_2SO_4	[137]
Co–N–C/Pt	≈0.45	5.6	10.8	≈48% after 4000 s	3.0 M CH_3OH + 1.0 M KOH	[143]
GDY@PtCu	≈0.65	0.70	0.82	≈95% after 5400 s	1.0 M CH_3OH + 0.5 M H_2SO_4	[145]
Pt/NGDY	≈0.47	1.4493	—	≈87% after 50 000 s	1.0 M CH_3OH + 1.0 M KOH	[146]
Pt/NGDY	≈0.69	0.296	29	>72% after 6000 s	1.0 M CH_3OH + 1.0 M H_2SO_4	[146]
Pt NW/PDDA-$Ti_3C_2T_x$	≈0.70	—	17.2	>90% after 2000 s	1.0 M CH_3OH + 0.5 M H_2SO_4	[147]
Ptc/$Ti_3C_2T_x$	≈0.4	7.32	38	≈56% after 3000 s	1.0 M CH_3OH + 1.0 M KOH	[148]
Pd/MXene	≈0.6	0.40	12.4	—	1.0 M CH_3OH + 1.0 M KOH	[149]
Pt–g-C_3N_4–CNT	≈0.5	—	19.45	≈60% after 3500 s	1.0 M CH_3OH + 0.5 M H_2SO_4	[154]
Pt_2Bi-A	≈0.52	4.611	—	≈35% after 10 000 s	1.0 M CH_3OH + 1.0 M KOH	[160]
PdNW/cCuO_x	≈0.66	≈0.55	6.14	≈96% after 3000 s	1.0 M CH_3OH + 1.0 M KOH	[161]
Pt_1/RuO_2	≈0.55	6.766	—	—	1.0 M CH_3OH + 0.1 M KOH	[173]
Single-Pt-atom-on-Ru	≈0.4	1.58	0.75	≈66% after 14 400 s	1.0 M CH_3OH + 0.1 M $HClO_4$	[75]

Note: Onset potential: potential vs RHE; MA: the activity per mass of Pt+Pd+Rh; Ru-ca-PtNi: Ru single atoms on the surface concavities of PtNi NPs; Pt NW/PDDA-$Ti_3C_2T_x$: Pt nanoworms grown on poly(diallyldimethyl ammonium chloride)-functionalized $Ti_3C_2T_x$ nanosheets.

to activate the reactants nor too strong to desorb the products. Scaling relations regarding the BE between the active sites and different adsorbed species open the possibility of using only a few descriptors to map the rate of catalytic reactions.[176] For complex catalysis reactions, it is hard to achieve a balance by breaking the restriction of the scaling relation between the multiple reaction intermediates which limits the optimization of catalysts.[177] The processes of MOR involve the adsorption/desorption of multiple reaction intermediates, which makes it urgent to unveil adsorption-energy scaling relations and build a paradigm guiding catalyst design.[178]

2) *Unveiling the Electrocatalytic MOR Process at the Molecular Level*: In situ and operando characterizations under real catalytic conditions should be explored to monitor the intricate chemical transformation and the evolution of active sites during the catalytic process, which is crucial to verify the proposed mechanisms, but are barely achieved yet. For example, the combination of in situ liquid phase-TEM with in situ microspectroscopic techniques to monitor the structure evolution of the active sites as well as the chemical reactions of adsorbed molecules. Online electrochemical mass spectrometry and in situ electron paramagnetic resonance are also powerful tools for the accurate detection of adsorbates and intermediates, which would take us one step closer to the fundamental nature of MOR. At present, the sensitivity, selectivity, and time resolution of the abovementioned techniques are needed to be further improved.
3) *Conquering the Limitations of DFT Calculations*: From the perspective of DFT calculations, it is hard to mimic the complex electrochemical system. Therefore, the catalyst model should be built accurately and based on the real state of active sites during the catalytic process. In addition, the effect of potential, the adsorption of water molecules, cations, and anions on the material surfaces should be carefully considered to ensure the results are reliable.

5.2. Rational Design of Advanced Electrocatalysts

1) *Modulating the Advanced Heterointerfaces to Break the Scaling Relations and Improve the Stability in the MOR*: Heterostructured electrocatalysts are distinguished by their structure inhomogeneity and complexity. Nørskov and co-workers have suggested that the optimized adsorption of the multiple intermediates at the abundant heterointerfaces makes it possible to break the scaling relation based on the first-principle calculations,[179] which is supported by many recent experimental studies.[180–182] The introduction of abundant interfaces would provide additional active sites for balancing intermediate adsorptions,[130,183] substantially improving the MOR

kinetics and alleviating the poisoning issues. Heterostructures, multimetal SACs, and HEAs have adjustable composition and interface chemistry, and are potential choices for high-performance MOR catalysts.[184] Moreover, enhancing the strong metal–support interactions or inducing spatial confinement effect at the heterointerfaces can efficiently prevent the catalysts from agglomeration and detachment.

2) *Exploring Catalysts based on Non-Platinum Group Metals*: Pt/Pd-based materials are the most intensively studied MOR electrocatalysts with an overpotential from 0.4–0.6 V (vs RHE) to trigger the reaction. However, nearly all the reported non-noble metal catalysts require a high potential of over 1.2 V, which is impractical for DMFCs because the theoretical potential for the cathodic reaction is 1.23 V. Wang et al. successfully synthesized a strain-stabilized $Ni(OH)_2$ nanoribbons (NR-$Ni(OH)_2$) with alternating 4- and 6-coordinated nickel edges atoms in a periodic manner.[185] Inspiringly, the prepared NR-$Ni(OH)_2$ exhibits outstanding MOR activity with an overpotential of 0.55 V and negligible CO poisoning.[186] Both experimental and theoretical investigations show that the four-coordinated Ni atom of NRc$Ni(OH)_2$ enables the electron transfer on the valence band near the Fermi energy level, which is forbidden in traditional six-coordinated Ni atom. The formed charge-transfer orbital finally facilitates the multi-electron transfer process during MOR. This work not only shows the importance of atomic coordination environment to catalytic nature but also indicates the feasibility of the application of non-precious metals for DMFCs that deserve specific attention.

Moreover, in practical DMFCs, the operation conditions are very different compared with the lab-scale test, and many more factors can affect the activity and stability of catalysts. It is urgent to build new criteria and evaluate directions to link the lab to the practical DMFCs applications.

Acknowledgements

This work was financially supported by the National Key R&D Program of China (No. 2022YFB4002503), the Natural Science Foundation of Zhejiang Province (No. LZ22B030006), and the National Natural Science Foundation of China (No. 52171224). J.W. acknowledges support from Zhejiang Province Postdoctoral Science Foundation (No. ZJ2022003).

Conflict of Interest

The authors declare no conflict of interest.

Keywords

direct methanol fuel cells, electrocatalysis, electrocatalysts, electrocatalytic mechanisms, methanol oxidation reactions

Received: November 28, 2022
Revised: January 23, 2023
Published online: May 28, 2023

[1] A. S. Aricò, V. Baglio, V. Antonucci, in *Electrocatalysis of Direct Methanol Fuel Cells*, (Eds: H. Zhang, H. Liu), Wiley-VCH, Weinheim, Germany **2009**, Ch. 17.
[2] F. Lyu, M. Cao, A. Mahsud, Q. Zhang, *J. Mater. Chem. A* **2020**, *8*, 15445.
[3] N. Kakati, J. Maiti, S. H. Lee, S. H. Jee, B. Viswanathan, Y. S. Yoon, *Chem. Rev.* **2014**, *114*, 12397.
[4] J. Zhang, S. Lu, Y. Xiang, S. P. Jiang, *ChemSusChem* **2020**, *13*, 2484.
[5] J. S. Li, R. L. Wei, X. Wang, Y. Zuo, X. Han, J. Arbiol, J. Llorca, Y. Y. Yang, A. Cabot, C. H. Cui, *Angew. Chem., Int. Ed.* **2020**, *59*, 20826.
[6] Y. Y. Tong, X. Yan, J. Liang, S. X. Dou, *Small* **2021**, *17*, 1904126.
[7] Z. Liu, Z. Zhao, B. Peng, X. Duan, Y. Huang, *J. Am. Chem. Soc.* **2020**, *142*, 17812.
[8] M. Borghei, J. Lehtonen, L. Liu, O. J. Rojas, *Adv. Mater.* **2018**, *30*, 1703691.
[9] U. Martinez, S. K. Babu, E. F. Holby, H. T. Chung, X. Yin, P. Zelenay, *Adv. Mater.* **2019**, *31*, 1806545.
[10] Y. Hu, M. Zhu, X. Luo, G. Wu, T. Chao, Y. Qu, F. Zhou, R. Sun, X. Han, H. Li, B. Jiang, Y. Wu, X. Hong, *Angew. Chem., Int. Ed.* **2021**, *60*, 6533.
[11] W. Zhang, Y. Yang, B. Huang, F. Lv, K. Wang, N. Li, M. Luo, Y. Chao, Y. Li, Y. Sun, *Adv. Mater.* **2019**, *31*, 1805833.
[12] X. Yang, Q. Wang, S. Qing, Z. Gao, X. Tong, N. Yang, *Adv. Energy Mater.* **2021**, *11*, 2100812.
[13] S. Han, Y. Ma, Q. Yun, A.-L. Wang, Q. Zhu, H. Zhang, C. He, J. Xia, X. Meng, L. Gao, W. Cao, Q. Lu, *Adv. Funct. Mater.* **2022**, *32*, 2208760.
[14] J. N. Tiwari, R. N. Tiwari, G. Singh, K. S. Kim, *Nano Energy* **2013**, *2*, 553.
[15] Q. Tan, C. Shu, J. Abbott, Q. Zhao, L. Liu, T. Qu, Y. Chen, H. Zhu, Y. Liu, G. Wu, *ACS Catal.* **2019**, *9*, 6362.
[16] S. L. Li, R. G. Ma, J. C. Hu, Z. C. Li, L. J. Liu, X. L. Wang, Y. Lu, G. E. Sterbinsky, S. H. Liu, L. Zheng, J. Liu, D. M. Liu, J. C. Wang, *Nat. Commun.* **2022**, *13*, 2916.
[17] Z. F. Liang, D. C. Jiang, X. Wang, M. Shakouri, T. Zhang, Z. J. Li, P. Y. Tang, J. Llorca, L. J. Liu, Y. P. Yuan, M. Heggen, R. E. Dunin-Borkowski, J. R. Morante, A. Cabot, J. Arbiol, *Adv. Funct. Mater.* **2021**, *31*, 2106349.
[18] J. S. Li, C. C. Xing, Y. Zhang, T. Zhang, M. C. Spadaro, Q. B. Wu, Y. N. Yi, S. L. He, J. Llorca, J. Arbiol, A. Cabot, C. H. Cui, *Small* **2021**, *17*, 2006623.
[19] J. Hao, J. Liu, D. Wu, M. Chen, Y. Liang, Q. Wang, L. Wang, X.-Z. Fu, J.-L. Luo, *Appl. Catal. B* **2021**, *281*, 119510.
[20] Y. Qi, Y. Zhang, L. Yang, Y. Zhao, Y. Zhu, H. Jiang, C. Li, *Nat. Commun.* **2022**, *13*, 4602.
[21] B. D. McNicol, D. A. J. Rand, K. R. Williams, *J. Power Sources* **1999**, *83*, 15.
[22] H. S. Wang, C. Wingender, H. Baltruschat, M. Lopez, M. T. Reetz, *J. Electroanal. Chem.* **2001**, *509*, 163.
[23] C.-S. Chen, F.-M. Pan, H.-J. Yu, *Appl. Catal. B* **2011**, *104*, 382.
[24] A. Yuda, A. Ashok, A. Kumar, *Catal. Rev.* **2022**, *64*, 126.
[25] Z. Jusys, J. Kaiser, R. Behm, *Langmuir* **2003**, *19*, 6759.
[26] T. H. Housmans, A. H. Wonders, M. T. Koper, *J. Phys. Chem. B* **2006**, *110*, 10021.
[27] A. Abd-El-Latif, H. Baltruschat, *J. Electroanal. Chem.* **2011**, *662*, 204.
[28] L. Gong, Z. Yang, K. Li, W. Xing, C. Liu, J. Ge, *J. Energy Chem.* **2018**, *27*, 1618.
[29] J. John, K. M. Hugar, J. Rivera-Melendez, H. A. Kostalik, E. D. Rus, H. Wang, G. W. Coates, H. D. Abruna, *J. Am. Chem. Soc.* **2014**, *136*, 5309.
[30] W. Chen, J. Cai, J. Yang, M. M. Sartin, Y.-X. Chen, *J. Electroanal. Chem.* **2017**, *800*, 89.
[31] D. Cao, G. Q. Lu, A. Wieckowski, S. A. Wasileski, M. Neurock, *J. Phys. Chem. B* **2005**, *109*, 11622.

[32] T. D. Jarvi, S. Sriramulu, E. M. Stuve, *J. Phys. Chem. B* **1997**, *101*, 3649.
[33] S. Sriramulu, T. D. Jarvi, E. M. Stuve, *J. Electroanal. Chem.* **1999**, *467*, 132.
[34] E. A. Batista, G. R. P. Malpass, A. J. Motheo, T. Iwasita, *Electrochem. Commun.* **2003**, *5*, 843.
[35] H. Kita, Y. Z. Gao, T. Nakato, H. Hattori, *J. Electroanal. Chem.* **1994**, *373*, 177.
[36] S. C. S. Lai, N. P. Lebedeva, T. H. M. Housmans, M. T. M. Koper, *Top. Catal.* **2007**, *46*, 320.
[37] R. Nagao, D. A. Cantane, F. H. B. Lima, H. Varela, *J. Phys. Chem. C* **2013**, *117*, 15098.
[38] R. Zeng, Y. Yang, T. Shen, H. Wang, Y. Xiong, J. Zhu, D. Wang, H. D. Abruna, *ACS Catal.* **2020**, *10*, 770.
[39] G. Wu, X. Han, J. Cai, P. Yin, P. Cui, X. Zheng, H. Li, C. Chen, G. Wang, X. Hong, *Nat. Commun.* **2022**, *13*, 4200.
[40] T. Yajima, H. Uchida, M. Watanabe, *J. Phys. Chem. B* **2004**, *108*, 2654.
[41] H.-X. Liu, N. Tian, M. P. Brandon, Z.-Y. Zhou, J.-L. Lin, C. Hardacre, W.-F. Lin, S.-G. Sun, *ACS Catal.* **2012**, *2*, 708.
[42] T. Iwasita, F. C. Nart, W. Vielstich, *Phys. Chem. Chem. Phys.* **1990**, *94*, 1030.
[43] D.-J. Chen, Y. J. Tong, *Angew. Chem., Int. Ed.* **2015**, *54*, 9394.
[44] Y.-W. Zhou, Y.-F. Chen, K. Jiang, Z. Liu, Z.-J. Mao, W.-Y. Zhang, W.-F. Lin, W.-B. Cai, *Appl. Catal. B* **2021**, *280*, 119393.
[45] F. P. Kong, X. Z. Liu, Y. J. Song, Z. Y. Qian, J. J. Li, L. Zhang, G. P. Yin, J. J. Wang, D. Su, X. L. Sun, *Angew. Chem., Int. Ed.* **2022**, *61*, e202207524.
[46] A. M. Jasim, S. E. Hoff, Y. Xing, *Electrochim. Acta* **2018**, *261*, 221.
[47] W. Liao, S. Zhou, Z. Wang, F. Liu, J. Cao, Q. Wang, *Fuel* **2022**, *308*, 122073.
[48] S. Lu, H. Li, J. Sun, Z. Zhuang, *Nano Res.* **2018**, *11*, 2058.
[49] Y. Qin, H. Zhuo, X. Liang, K. Yu, Y. Wang, D. Gao, X. Zhang, *Dalton Trans.* **2019**, *48*, 10313.
[50] W. Huang, H. Wang, J. Zhou, J. Wang, P. N. Duchesne, D. Muir, P. Zhang, N. Han, F. Zhao, M. Zeng, *Nat. Commun.* **2015**, *6*, 10035.
[51] X. T. Li, H. Lei, C. Yang, Q. B. Zhang, *J. Power Sources* **2018**, *396*, 64.
[52] D. S. Mekazni, R. M. Aran-Ais, A. Ferre-Vilaplana, E. Herrero, *ACS Catal.* **2022**, *12*, 1965.
[53] A.-X. Yin, X.-Q. Min, Y.-W. Zhang, C.-H. Yan, *J. Am. Chem. Soc.* **2011**, *133*, 3816.
[54] E. Herrero, K. Franaszczuk, A. Wieckowski, *J. Phys. Chem.* **1994**, *98*, 5074.
[55] S. Sriramulu, T. Jarvi, E. Stuve, *J. Electroanal. Chem.* **1999**, *467*, 132.
[56] Q. Feng, S. Zhao, D. He, S. Tian, L. Gu, X. Wen, C. Chen, Q. Peng, D. Wang, Y. Li, *J. Am. Chem. Soc.* **2018**, *140*, 2773.
[57] P. Ferrin, M. Mavrikakis, *J. Am. Chem. Soc.* **2009**, *131*, 14381.
[58] M. J. S. Farias, W. Cheuquepan, A. A. Tanaka, J. M. Feliu, *ACS Catal.* **2020**, *10*, 543.
[59] P. Waszczuk, G. Q. Lu, A. Wieckowski, C. Lu, C. Rice, R. I. Masel, *Electrochim. Acta* **2002**, *47*, 3637.
[60] D. Y. Chung, K.-J. Lee, Y.-E. Sung, *J. Phys. Chem. C* **2016**, *120*, 9028.
[61] B. Hammer, J. K. Nørskov, *Adv. Catal.* **2000**, *45*, 71.
[62] S. Jiao, X. Fu, H. Huang, *Adv. Funct. Mater.* **2022**, *32*, 2107651.
[63] F. Kong, X. Liu, Y. Song, Z. Qian, J. Li, L. Zhang, G. Yin, J. Wang, D. Su, X. Sun, *Angew. Chem., Int. Ed.* **2022**, *61*, e202207524.
[64] R. Mancharan, J. B. Goodenough, *J. Phys. Chem.* **1992**, *2*, 875.
[65] Z. Liu, X. Y. Ling, X. Su, J. Y. Lee, *J. Phys. Chem. B* **2004**, *108*, 8234.
[66] A. M. Hofstead-Duffy, D.-J. Chen, S.-G. Sun, Y. J. Tong, *J. Phys. Chem.* **2012**, *22*, 5205.
[67] L. Lai, G. Yang, Q. Zhang, H. Yu, F. Peng, *J. Power Sources* **2021**, *509*, 230397.
[68] Y. Zhao, X. Li, J. M. Schechter, Y. Yang, *RSC Adv.* **2016**, *6*, 5384.
[69] H.-S. Chen, T. M. Benedetti, J. Lian, S. Cheong, P. B. O'Mara, K. O. Sulaiman, C. H. Kelly, R. W. Scott, J. J. Gooding, R. D. Tilley, *ACS Catal.* **2021**, *11*, 2235.
[70] M. Qiao, F.-Y. Meng, H. Wu, Y. Wei, X.-F. Zeng, J.-X. Wang, *Small* **2022**, *18*, 2204720.
[71] F. Y. Chen, Z. Y. Wu, Z. Adler, H. T. Wang, *Joule* **2021**, *5*, 1704.
[72] M. Li, Z. Zhao, W. Zhang, M. Luo, L. Tao, Y. Sun, Z. Xia, Y. Chao, K. Yin, Q. Zhang, L. Gu, W. Yang, Y. Yu, G. Lu, S. Guo, *Adv. Mater.* **2021**, *33*, 2103762.
[73] T. J. Wang, F. M. Li, H. Huang, S. W. Yin, P. Chen, P. J. Jin, Y. Chen, *Adv. Funct. Mater.* **2020**, *30*, 2000534.
[74] W. Chen, J. Xue, Y. Bao, L. Feng, *Chem. Eng. J.* **2020**, *381*, 122752.
[75] A. R. Poerwoprajitno, L. Gloag, J. Watt, S. Cheong, X. Tan, H. Lei, H. A. Tahini, A. Henson, B. Subhash, N. M. Bedford, B. K. Miller, P. B. O'Mara, T. M. Benedetti, D. L. Huber, W. Zhang, S. C. Smith, J. J. Gooding, W. Schuhmann, R. D. Tilley, *Nat. Catal.* **2022**, *5*, 231.
[76] Y. Yang, Y. Xiong, R. Zeng, X. Lu, M. Krumov, X. Huang, W. Xu, H. Wang, F. J. DiSalvo, J. D. Brock, D. A. Muller, H. D. Abruna, *ACS Catal.* **2021**, *11*, 1136.
[77] G. Han, M. Li, H. Liu, W. Zhang, L. He, F. Tian, Y. Liu, Y. Yu, W. Yang, S. Guo, *Adv. Mater.* **2022**, *34*, 2202943.
[78] O. H. Han, K. S. Han, C. W. Shin, J. Lee, S.-S. Kim, M. S. Um, H.-I. Joh, S.-K. Kim, H. Y. Ha, *Angew. Chem., Int. Ed.* **2012**, *51*, 3842.
[79] L. Chong, J. Wen, J. Kubal, F. G. Sen, J. Zou, J. Greeley, M. Chan, H. Barkholtz, W. Ding, D.-J. Liu, *Science* **2018**, *362*, 1276.
[80] D. Li, C. Wang, D. S. Strmcnik, D. V. Tripkovic, X. Sun, Y. Kang, M. Chi, J. D. Snyder, D. van der Vliet, Y. Tsai, V. R. Stamenkovic, S. Sun, N. M. Markovic, *Energy Environ. Sci.* **2014**, *7*, 4061.
[81] L. Huang, X. Zhang, Q. Wang, Y. Han, Y. Fang, S. Dong, *J. Am. Chem. Soc.* **2018**, *140*, 1142.
[82] F. Taufany, C.-J. Pan, F.-J. Lai, H.-L. Chou, L. S. Sarma, J. Rick, J.-M. Lin, J.-F. Lee, M.-T. Tang, B.-J. Hwang, *Chemistry* **2013**, *19*, 905.
[83] F. Liu, J. Y. Lee, W. J. Zhou, *Small* **2006**, *2*, 121.
[84] H. Wang, Y. Wu, X. Luo, L. Jiao, X. Wei, W. Gu, D. Du, Y. Lin, C. Zhu, *Nanoscale* **2019**, *11*, 10575.
[85] S. Zhang, H. Rong, T. Yang, B. Bai, J. Zhang, *Chemistry* **2020**, *26*, 4025.
[86] R. Zhu, Y. Yu, R. Yu, J. Lai, J. C.-Y. Jung, S. Zhang, Y. Zhao, J. Zhang, Z. Xia, *J. Colloid Interface Sci.* **2022**, *625*, 493.
[87] R. B. Araujo, D. Martin-Yerga, E. C. dos Santos, A. Cornell, L. G. M. Pettersson, *Electrochim. Acta* **2020**, *360*, 136954.
[88] W. Wang, X. W. Chen, X. Zhang, J. Y. Ye, F. Xue, C. Zhen, X. Y. Liao, H. Q. Li, P. T. Li, M. C. Liu, Q. Kuang, Z. X. Xie, S. F. Xie, *Nano Energy* **2020**, *71*, 104623.
[89] Y.-l. Qin, Y.-c. Liu, F. Liang, L.-m. Wang, *ChemSusChem* **2015**, *8*, 260.
[90] G. Sheng, J. Chen, H. Ye, Z. Hu, X.-Z. Fu, R. Sun, W. Huang, C.-P. Wong, *J. Colloid Interface Sci.* **2018**, *522*, 264.
[91] Y. Qi, T. Bian, S.-I. Choi, Y. Jiang, C. Jin, M. Fu, H. Zhang, D. Yang, *Chem. Commun.* **2014**, *50*, 560.
[92] C. Xu, Y. Liu, J. Wang, H. Geng, H. Qiu, *ACS Appl. Mater. Interfaces* **2011**, *3*, 4626.
[93] Y. Wang, H.-Z. Yu, J. Ying, G. Tian, Y. Liu, W. Geng, J. Hu, Y. Lu, G.-G. Chang, K. I. Ozoemena, C. Janiak, X.-Y. Yang, *Chemistry* **2021**, *27*, 9124.
[94] S. Guo, S. Zhang, X. Sun, S. Sun, *J. Am. Chem. Soc.* **2011**, *133*, 15354.
[95] H. Wang, K. Zhang, J. Qiu, J. Wu, J. Shao, H. Wang, Y. Zhang, J. Han, Y. Zhang, L. Yan, *Nanoscale* **2020**, *12*, 9824.
[96] L. Wang, X. L. Tian, Y. Xu, S. Zaman, K. Qi, H. Liu, B. Y. Xia, *J. Mater. Chem. A* **2019**, *7*, 13090.
[97] M. Qiao, H. Wu, F.-Y. Meng, Z. Zhuang, J.-X. Wang, *Small* **2022**, *18*, 2106643.
[98] X. B. Xie, G. H. Gao, S. D. Kang, T. Shibayama, Y. H. Lei, D. Y. Gao, L. T. Cai, *Adv. Mater.* **2015**, *27*, 5573.

[99] T. Zhang, Y. Q. Sun, X. J. Li, X. Y. Li, D. L. Liu, G. Q. Liu, C. C. Li, H. J. Fan, Y. Li, *Small Methods* **2020**, *4*, 1900709.
[100] Z. H. Xing, J. Li, S. Wang, C. L. Su, H. L. Jin, *Nano Res.* **2022**, *15*, 3866.
[101] J. N. Xue, Z. Hu, H. Li, Y. Zhang, C. Liu, M. Li, Q. H. Yang, S. Hu, *Nano Res.* **2022**, *15*, 8819.
[102] Z. M. Cui, H. Chen, M. T. Zhao, D. Marshall, Y. C. Yu, H. Abruna, F. J. DiSalvo, *J. Am. Chem. Soc.* **2014**, *136*, 10206.
[103] Y. Kang, J. B. Pyo, X. Ye, T. R. Gordon, C. B. Murray, *ACS Nano* **2012**, *6*, 5642.
[104] M. Iqbal, Y. V. Kaneti, J. Kim, B. Yuliarto, Y. M. Kang, Y. Bando, Y. Sugahara, Y. Yamauchi, *Small* **2019**, *15*, 1804378.
[105] X. Zhao, Q. M. Liu, Q. X. Li, L. Y. Chen, L. Mao, H. Y. Wang, S. W. Chen, *Chem. Eng. J.* **2020**, *400*, 125744.
[106] X. L. Tian, L. J. Wang, P. L. Deng, Y. Chen, B. Y. Xia, *J. Energy Chem.* **2017**, *26*, 1067.
[107] J. T. L. Gamler, H. M. Ashberry, S. E. Skrabalak, K. M. Koczkur, *Adv. Mater.* **2018**, *30*, 1801563.
[108] Y. G. Yao, Q. Dong, A. Brozena, J. Luo, J. W. Miao, M. F. Chi, C. Wang, I. G. Kevrekidis, Z. J. Ren, J. Greeley, G. F. Wang, A. Anapolsky, L. B. Hu, *Science* **2022**, *376*, eabn3103.
[109] L. Tao, M. Sun, Y. Zhou, M. Luo, F. Lv, M. Li, Q. Zhang, L. Gu, B. Huang, S. Guo, *J. Am. Chem. Soc.* **2022**, *144*, 10582.
[110] E. P. George, D. Raabe, R. O. Ritchie, *Nat. Rev. Mater.* **2019**, *4*, 515.
[111] H. Li, Y. Han, H. Zhao, W. Qi, D. Zhang, Y. Yu, W. Cai, S. Li, J. Lai, B. Huang, L. Wang, *Nat. Commun.* **2020**, *11*, 5437.
[112] W. Chen, S. Luo, M. Sun, X. Wu, Y. Zhou, Y. Liao, M. Tang, X. Fan, B. Huang, Z. Quan, *Adv. Mater.* **2022**, *34*, 2206276.
[113] A.-L. Wang, H.-C. Wan, H. Xu, Y.-X. Tong, G.-R. Li, *Electrochim. Acta* **2014**, *127*, 448.
[114] X. Chen, C. Si, Y. Gao, J. Frenzel, J. Sun, G. Eggeler, Z. Zhang, *J. Power Sources* **2015**, *273*, 324.
[115] M. Li, K. Duanmu, C. Wan, T. Cheng, L. Zhang, S. Dai, W. Chen, Z. Zhao, P. Li, H. Fei, *Nat. Catal.* **2019**, *2*, 495.
[116] L. Chen, X. Liang, D. Wang, Z. Yang, C.-T. He, W. Zhao, J. Pei, Y. Xue, *ACS Appl. Mater. Interfaces* **2022**, *14*, 27814.
[117] M. Oezaslan, F. Hasche, P. Strasser, *J. Phys. Chem. Lett.* **2013**, *4*, 3273.
[118] M. Li, Z. Zhao, Z. Xia, M. Luo, Q. Zhang, Y. Qin, L. Tao, K. Yin, Y. Chao, L. Gu, W. Yang, Y. Yu, G. Lu, S. Guo, *Angew. Chem., Int. Ed.* **2021**, *60*, 8243.
[119] S. Das, J. Perez-Ramirez, J. Gong, N. Dewangan, K. Hidajat, B. C. Gates, S. Kawi, *Chem. Soc. Rev.* **2020**, *49*, 2937.
[120] A. R. Hernandez, E. M. A. Estrada, A. Ezeta, M. E. Manriquez, *Electrochim. Acta* **2019**, *327*, 134977.
[121] R. Wang, H. Wang, F. Luo, S. Liao, *Electrochem. Energy Rev.* **2018**, *1*, 324.
[122] H. Xie, S. Chen, J. Liang, T. Wang, Z. Hou, H.-L. Wang, G. Chai, Q. Li, *Adv. Funct. Mater.* **2021**, *31*, 2100883.
[123] H. Z. Yang, J. Zhang, K. Sun, S. Z. Zou, J. Y. Fang, *Angew. Chem., Int. Ed.* **2010**, *49*, 6848.
[124] M.-X. Chen, X. Luo, T.-W. Song, B. Jiang, H.-W. Liang, *J. Phys. Chem. Lett.* **2022**, *13*, 3549.
[125] L. Bu, N. Zhang, S. Guo, X. Zhang, J. Li, J. Yao, T. Wu, G. Lu, J.-Y. Ma, D. Su, *Science* **2016**, *354*, 1410.
[126] S. Luo, L. Zhang, Y. Liao, L. Li, Q. Yang, X. Wu, X. Wu, D. He, C. He, W. Chen, *Adv. Mater.* **2021**, *33*, 2008508.
[127] X. Yang, X. Tong, X. Liu, K. Li, N. Yang, *Electrochem. Commun.* **2021**, *123*, 106917.
[128] T. He, W. Wang, F. Shi, X. Yang, X. Li, J. Wu, Y. Yin, M. Jin, *Nature* **2021**, *598*, 76.
[129] Y. Wang, X. Zheng, D. Wang, *Nano Res.* **2022**, *15*, 1730.
[130] G. Zhao, Y. Jiang, S.-X. Dou, W. Sun, H. Pan, *Sci. Bull.* **2020**, *66*, 85.
[131] G. Chen, Z. Dai, L. Sun, L. Zhang, S. Liu, H. Bao, J. Bi, S. Yang, F. Ma, *J. Mater. Chem. A* **2019**, *7*, 6562.
[132] H. Huang, Q. Chen, M. He, X. Sun, X. Wang, *J. Power Sources* **2013**, *239*, 189.
[133] Y. Huang, H. Huang, Q. Gao, C. Gan, Y. Liu, Y. Fang, *Electrochim. Acta* **2014**, *149*, 34.
[134] J. Li, Y. Chang, D. Li, L. Feng, B. Zhang, *Chem. Commun.* **2021**, *57*, 7035.
[135] Q. Tan, H. Zhu, S. Guo, Y. Chen, T. Jiang, C. Shu, S. Chong, B. Hultman, Y. Liu, G. Wu, *Nanoscale* **2017**, *9*, 12565.
[136] Y. Zhao, S. Nie, H. Wang, J. Tian, Z. Ning, X. Li, *J. Power Sources* **2012**, *218*, 320.
[137] L. Tao, Y. Shi, Y.-C. Huang, R. Chen, Y. Zhang, J. Huo, Y. Zou, G. Yu, J. Luo, C.-L. Dong, *Nano Energy* **2018**, *53*, 604.
[138] Y. Sun, C. Du, G. Han, Y. Qu, L. Du, Y. Wang, G. Chen, Y. Gao, G. Yin, *Electrochim. Acta* **2016**, *212*, 313.
[139] M. Li, Q. Jiang, M. Yan, Y. Wei, J. Zong, J. Zhang, Y. Wu, H. Huang, *ACS Sustainable Chem. Eng.* **2018**, *6*, 6644.
[140] D. Chen, Z. He, S.-e. Pei, L.-a. Huang, H. Shao, Y. Jin, J. Wang, *J. Alloys Compd.* **2019**, *785*, 781.
[141] L. Yang, G. Li, R. Ma, S. Hou, J. Chang, M. Ruan, W. Cai, Z. Jin, W. Xu, G. Wang, J. Ge, C. Liu, W. Xing, *Nano Res.* **2021**, *14*, 2853.
[142] B. Xiong, Y. Zhou, Y. Zhao, J. Wang, X. Chen, R. O'Hayre, Z. Shao, *Carbon* **2013**, *52*, 181.
[143] J. F. Ruan, Y. P. Chen, G. Q. Zhao, P. Li, B. X. Zhang, Y. Z. Jiang, T. Y. Ma, H. G. Pan, S. X. Dou, W. P. Sun, *Small* **2022**, *18*, 2107067.
[144] G. Li, Y. Li, H. Liu, Y. Guo, Y. Li, D. Zhu, *Chem. Commun.* **2010**, *46*, 3256.
[145] H. Pan, Z. Jiang, Z. Zuo, F. He, F. Wang, L. Li, Q. Chang, B. Guan, Y. Li, *Nano Today* **2021**, *39*, 101213.
[146] L. Hui, Y. Xue, C. Xing, Y. Liu, Y. Du, Y. Fang, H. Yu, B. Huang, Y. Li, *Adv. Sci.* **2022**, *9*, 2104991.
[147] C. Yang, Q. Jiang, H. Huang, H. He, L. Yang, W. Li, *ACS Appl. Mater. Interfaces* **2020**, *12*, 23822.
[148] J. Zhu, L. Xia, R. Yu, R. Lu, J. Li, R. He, Y. Wu, W. Zhang, X. Hong, W. Chen, Y. Zhao, L. Zhou, L. Mai, Z. Wang, *J. Am. Chem. Soc.* **2022**, *144*, 15529.
[149] Z. Lang, Z. Zhuang, S. Li, L. Xia, Y. Zhao, Y. Zhao, C. Han, L. Zhou, *ACS Appl. Mater. Interfaces* **2019**, *12*, 2400.
[150] W. Zhang, H. Huang, F. Li, K. Deng, X. Wang, *J. Mater. Chem. A* **2014**, *2*, 19084.
[151] C.-Z. Li, Z.-B. Wang, X.-L. Sui, L.-M. Zhang, D.-M. Gu, *Carbon* **2015**, *93*, 105.
[152] C.-Z. Li, Z.-B. Wang, X.-L. Sui, L.-M. Zhang, D.-M. Gu, S. Gu, *J. Mater. Chem. A* **2014**, *2*, 20139.
[153] D. Fang, L. Yang, G. Yang, G. Yi, Y. Feng, P. Shao, H. Shi, K. Yu, D. You, X. Luo, *Int. J. Hydrogen Energy* **2020**, *45*, 21483.
[154] W. Zhang, Q. Yao, G. Jiang, C. Li, Y. Fu, X. Wang, A. Yu, Z. Chen, *ACS Catal.* **2019**, *9*, 11603.
[155] W. Chen, S. Luo, M. Sun, M. Tang, X. Fan, Y. Cheng, X. Wu, Y. Liao, B. Huang, Z. Quan, *Small* **2022**, *18*, 2107803.
[156] Q. Fu, F. Yang, X. Bao, *Acc. Chem. Res.* **2013**, *46*, 1692.
[157] Y. Li, S. Li, M. Baeumer, E. A. Ivanova-Shor, L. V. Moskaleva, *ACS Catal.* **2020**, *10*, 3164.
[158] Z. Lyu, X.-G. Zhang, Y. Wang, K. Liu, C. Qiu, X. Liao, W. Yang, Z. Xie, S. Xie, *Angew. Chem., Int. Ed.* **2021**, *60*, 16093.
[159] H. Yan, C. Yang, W.-P. Shao, L.-H. Cai, W.-W. Wang, Z. Jin, C.-J. Jia, *Nat. Commun.* **2019**, *10*, 3470.
[160] X. Wang, M. Xie, F. Lyu, Y.-M. Yiu, Z. Wang, J. Chen, L.-Y. Chang, Y. Xia, Q. Zhong, M. Chu, *Nano Lett.* **2020**, *20*, 7751.
[161] Z. Chen, Y. Liu, C. Liu, J. Zhang, Y. Chen, W. Hu, Y. Deng, *Small* **2020**, *16*, 1904964.
[162] R. Z. Li, D. S. Wang, *Nano Res.* **2022**, *15*, 6888.

[163] J. Xia, B. Wang, J. Di, Y. Li, S.-Z. Yang, H. Li, S. Guo, *Mater. Today* **2022**, *53*, 217.
[164] L. Wang, D. Wang, Y. Li, *Carbon Energy* **2022**, *4*, 1021.
[165] P. Zhu, X. Xiong, D. Wang, *Nano Res.* **2022**, *15*, 5792.
[166] Y. Liang, J. Wei, X. Zhang, J. Zhang, S. P. Jiang, H. Wang, *ChemCatChem* **2016**, *8*, 1901.
[167] L.-M. Zhang, X.-L. Sui, L. Zhao, J.-J. Zhang, D.-M. Gu, Z.-B. Wang, *Carbon* **2016**, *108*, 561.
[168] T. Wu, M.-Y. Han, Z. J. Xu, *ACS Nano* **2022**, *16*, 8531.
[169] T. Frelink, W. Visscher, J. A. R. Vanveen, *J. Electroanal. Chem.* **1995**, *382*, 65.
[170] K. Bergamaski, A. L. N. Pinheiro, E. Teixeira-Neto, F. C. Nart, *J. Phys. Chem. B* **2006**, *110*, 19271.
[171] A. Cuesta, *J. Am. Chem. Soc.* **2006**, *128*, 13332.
[172] Y. T. Kim, K. Ohshima, K. Higashimine, T. Uruga, M. Takata, H. Suematsu, T. Mitani, *Angew. Chem., Int. Ed.* **2006**, *45*, 407.
[173] Z. Zhang, J. Liu, J. Wang, Q. Wang, Y. Wang, K. Wang, Z. Wang, M. Gu, Z. Tang, J. Lim, T. Zhao, F. Ciucci, *Nat. Commun.* **2021**, *12*, 5235.
[174] X. W. Bai, X. H. Zhao, Y. H. Zhang, C. Y. Ling, Y. P. Zhou, J. L. Wang, Y. Y. Liu, *J. Am. Chem. Soc.* **2022**, *144*, 17140.
[175] J. Yang, H. Qi, A. Li, X. Liu, X. Yang, S. Zhang, Q. Zhao, Q. Jiang, Y. Su, L. Zhang, J.-F. Li, Z.-Q. Tian, W. Liu, A. Wang, T. Zhang, *J. Am. Chem. Soc.* **2022**, *144*, 12062.
[176] A. J. Medford, A. Vojvodic, J. S. Hummelshøj, J. Voss, F. Abild-Pedersen, F. Studt, T. Bligaard, A. Nilsson, J. K. Nørskov, *J. Catal.* **2015**, *328*, 36.
[177] Z.-J. Zhao, S. Liu, S. Zha, D. Cheng, F. Studt, G. Henkelman, J. Gong, *Nat. Rev. Mater.* **2019**, *4*, 792.
[178] Z.-F. Huang, J. Song, S. Dou, X. Li, J. Wang, X. Wang, *Matter* **2019**, *1*, 1494.
[179] J. H. Montoya, C. Tsai, A. Vojvodic, J. K. Nørskov, *ChemSusChem* **2015**, *8*, 2180.
[180] P. Wang, F. Chang, W. Gao, J. Guo, G. Wu, T. He, P. Chen, *Nat. Chem.* **2017**, *9*, 64.
[181] C. Mao, J. Wang, Y. Zou, G. Qi, J. Y. Y. Loh, T. Zhang, M. Xia, J. Xu, F. Deng, M. Ghoussoub, *J. Am. Chem. Soc.* **2020**, *142*, 17403.
[182] G. Zhao, P. Li, N. Cheng, S. X. Dou, W. Sun, *Adv. Mater.* **2020**, *32*, 2000872.
[183] G. Zhao, K. Rui, S. X. Dou, W. Sun, *Adv. Funct. Mater.* **2018**, *28*, 1803291.
[184] R. Li, D. Wang, *Adv. Energy Mater.* **2022**, *12*, 2103564.
[185] X. P. Wang, H. J. Wu, S. B. Xi, W. S. V. Lee, J. Zhang, Z. H. Wu, J. O. Wang, T. D. Hu, L. M. Liu, Y. Han, S. W. Chee, S. C. Ning, U. Mirsaidov, Z. B. Wang, Y. W. Zhang, A. Borgna, J. Wang, Y. H. Du, Z. G. Yu, S. J. Pennycook, J. M. Xue, *Energy Environ. Sci.* **2020**, *13*, 229.
[186] X. Wang, S. Xi, W. S. V. Lee, P. Huang, P. Cui, L. Zhao, W. Hao, X. Zhao, Z. Wang, H. Wu, *Nat. Commun.* **2020**, *11*, 4647.

Jianmei Wang is currently a postdoctoral fellow at the School of Materials Science and Engineering, Zhejiang University. She received her Ph.D. in 2021 from the School of Life and Environmental Sciences, Deakin University. Her research interests include design SERS active nano-/microelectrodes for real-time observation of interfacial molecular chemistry and synthesis of advanced electrocatalysts for energy conversion.

Wenping Sun is a professor at the School of Materials Science and Engineering, Zhejiang University. He received his B.S. in 2008 and Ph.D. in 2013 in materials science from the University of Science and Technology of China (USTC). His research expertise includes electrocatalysis, fuel cells, and batteries, with a specific focus on the rational design of novel materials and structures, advanced characterization techniques, and fundamental understanding of related electrochemical processes.